Back arc extension and collision : an experimental approach of the tectonics of Asia

Marc Fournier, Laurent Jolivet, Philippe Davy, Jean-Charles Thomas

Back arc extension and collision:

An experimental approach of the tectonics of Asia

Marc Fournier[1*], Laurent Jolivet[1], Philippe Davy[2], Jean-Charles Thomas[3]

[1] CNRS UMR 7072, Laboratoire de Tectonique, Université Pierre et Marie Curie, Case 129, 4 place Jussieu, 75252 Paris Cedex 05, France

[2] Centre Armoricain d'Etude Structurale des Socles, Université de Rennes 1, 35042 Rennes Cedex, France

[3] Laboratoire de Géophysique Interne et Tectonophysique, BP 53, 38041 Grenoble Cedex 9, France

[*] Corresponding author: marc.fournier@lgs.jussieu.fr Fax: (33) 1-44-27-50-85

Abstract. The deformation of the eastern Asian lithosphere during the first part of the India-Asia collision was dominated by subduction-related extension interacting with far effects of the collision. In order to investigate the role of large-scale extension in collision tectonics, we performed analogue experiments of indentation with a model of lithosphere subjected to extension. We used a 3-layers rheological model of continental lithosphere resting upon an asthenosphere of low viscosity and strained along its southern boundary by a rigid indenter progressing northward. The lithosphere model was scaled to be gravitationally unstable and to spread under its own weight, so that extension occurred in the whole model. The eastern boundary was free or weakly confined and always allowed eastward spreading of the model. We studied the pattern of deformation for different boundary conditions. The experimental pattern of deformation includes a thickened zone in front of the indenter, a major NE trending

left-lateral shear zone starting from the NW corner of the indenter, antithetic N-S right-lateral shear zones more or less developed to the east of the indenter, and a purely extensional domain in the southeastern part of the model. In this domain, graben opening is driven by gravitational spreading, whereas it is driven by gravitational spreading and indentation in the north-eastern part where grabens opened along strike-slip faults. The results are compared to the Oligo-Miocene deformation pattern of Asia consecutive to the collision of India. Our experiments bring a physical basis to models which favour distributed deformation within a slowly extruded wide region extending from the Baikal Rift to the Okhotsk Sea and to SE Asia and Indonesia. In this large domain, the opening of back arc basins (Japan Sea, Okinawa Trough, South China Sea) and continental grabens (North China grabens) have been associated with ~N-S trending right-lateral strike-slip faults, which accommodated the northward penetration of India into Eurasia.

Key words: continental deformation, experimental tectonics, tectonics of Asia, collision, extension

Abbreviated title: back arc extension and collision tectonics in Asia

Introduction

Since Argand (1924) and Molnar and Tapponnier (1975) related the deformation of Asia to the collision of India which started 50 Ma ago, numerous analogue and numerical experiments were performed to characterise the deformation of the Asian continental lithosphere under various conditions of lateral constraint (Tapponnier and Molnar, 1976; England and McKenzie, 1982; Tapponnier et al., 1982; Vilotte et al., 1982, 1984, 1986; Houseman and England, 1986, 1993, 1996; Davy and Cobbold, 1988; Peltzer and Tapponnier, 1988; Shemenda and Grokholski, 1992; Martinod and Davy, 1994; Kong and Bird, 1996; England and Molnar, 1997; Holt et al., 2000; Flesch et al., 2001). The debate mainly focused

on the geometry of deformation around the collision zone, the degree of localization of the deformation, and the amount of deformation taken up by thickening and lateral extrusion (England et al., 1985; England and Houseman, 1986; Tapponnier et al., 1986; Cobbold and Davy, 1988; Dewey et al., 1989; England and Molnar, 1990; Burchfiel and Royden, 1991; Le Pichon et al., 1992; Houseman and England, 1993; Davy et al., 1995). The observations used to argue in favour of one or the other models were mostly related to the recent and active deformation, i.e., Quaternary fault slip rates (Molnar et al., 1987; Avouac and Tapponnier, 1993; Peltzer and Saucier, 1996; England and Molnar, 1997), seismic strain rates (Molnar and Deng, 1984; Holt et al., 1991, 1995; Holt and Haines, 1993; Qin et al., 2002), and space geodetic measurements (Molnar and Gipson, 1996; Heki, 1996; Crétaux et al., 1998; Heki et al., 1999; Larson et al., 1999; Chamot-Rooke and Le Pichon, 1999; Holt et al., 2000; Shen et al., 2000; Flesch et al., 2001; Wang et al., 2001). However, the deformation pattern of Asia drastically changed around the Middle Miocene because the boundary conditions in eastern and south-eastern Asia changed at that time. From the Eocene to the Middle Miocene, extension largely prevailed on the eastern and south-eastern margins of Asia where major marginal basins opened above the western Pacific subduction zones. Rather than stress free, the eastern boundary of Asia was subjected to dynamic extension related to subduction. Several important questions are worth asking about the Oligo-Miocene deformation: (1) how far from the Indian indenter has the Asian lithosphere been deformed? Was the deformation only concentrated around Tibet or was it felt much further as far as the northern Sea of Okhotsk (Kimura and Tamaki, 1986; Jolivet et al., 1990; Worral et al., 1996)? (2) How much was the opening of marginal basins of eastern Asia shaped by the collision process?

We performed analogue experiments of indentation to understand the role of extension in collision tectonics. Our prime interest was to study the deformation of continental margins subjected to subduction-related extension during indentation. The role of retreating

subduction was experimentally simulated by using a gravitationally unstable plate model. In the following, we first present a review of the extensional deformation in Asia since the Eocene to justify the rheology of the models and the boundary conditions of the experiments. We then describe four experiments with different boundary conditions. We discuss the kinematics and geometry of deformation with respect to boundary conditions, paying attention to extensional deformation. We finally compare the deformation of the Asian margins to the experiments.

1. From extension to compression on the Asian margins

1.1. Extension in Asia since the Eocene

Far from the collision zone, the Asian lithosphere underwent extension during the Cenozoic (Figure 1a). From the Eocene to the Middle Miocene, the eastern and south-eastern Asian margins were affected by back-arc extension. Basins floored with oceanic crust opened: the Celebes Sea in the Eocene (Weissel, 1980; Silver et al., 1983a; Silver and Rangin, 1991a), the South China Sea in the Oligo-Miocene (Taylor and Hayes, 1980; Briais et al., 1993), the Japan and Okhotsk seas from the Late Oligocene to the Middle Miocene (Tamaki, 1988, Tamaki et al., 1992; Worrall et al., 1996), and the Sulu Sea in the Early Miocene (Silver and Rangin, 1991b). Basin systems in Sumatra, Sunda shelf, Borneo, Gulf of Thailand and Malaysia also opened during the Eocene and Oligocene (Hamilton, 1979, Daly et al., 1991). The opening of marginal basins ceased during the Middle Miocene and resumed in the Okinawa Trough in the late Miocene (Sibuet et al., 1995, 1998). Several models have been proposed to relate back-arc extension and spreading to subduction, including secondary induced asthenospheric convection (McKenzie, 1969), mass upwelling of the asthenosphere (Karig, 1971, Tatsumi et al., 1989), gravity or eastward asthenospheric flow acting on a dense

subducting slab (Molnar and Atwater, 1978, Uyeda and Kanamori, 1979), and collapse of a thickened continental margin (Le Pichon, 1982; Faccenna et al., 1996, 1999).

Extension was not restricted to the Asian margins and also affected the inland part of the continent. Since Eocene time, northern China experiences distributed extension over the multi-rifted North China Basin (Figure 1a; Hellinger et al., 1985, Hong et al., 1985, Chen and Nabelek, 1988, Tian et al., 1992; Allen et al., 1997) and in the Hetao, Yinchuan and Weihe graben systems surrounding the Ordos block (Ma and Wu, 1987, Wang, 1987, Bellier et al., 1988). Extension in the Shanxi graben system, east of the Ordos block, was initiated during the Pliocene (Xu and Ma, 1992). In the Baikal region, extension started during the Oligocene (Tapponnier and Molnar, 1979; Hutchinson et al., 1992; Deverchère et al., 1993), and Windley and Allen (1993) proposed that a mantle plume was responsible for the extension in this area.

Extension also occurred near the collision zone in relation with the growing topography in front of the Indian indenter. It is currently active in the Himalayas and in Tibet (Molnar and Tapponnier, 1978; Tapponnier et al., 1981; Molnar and Chen, 1983; Burg et al., 1984; Burchfiel and Royden, 1985; Armijo et al., 1986, 1989; Burchfiel et al., 1992), where it started in the Middle or Late Miocene (Mercier et al., 1987; Pan and Kidd, 1992; Coleman and Hodges, 1995). Bird (1991) proposed a model of extension in Tibet driven by lateral extrusion of the lower crust under the topographic load.

1.2. Extension associated with right-lateral strike-slip faulting in eastern Asia

The opening of the main marginal basins and continental grabens of eastern Asia, from the Okhotsk Sea to the South China Sea and to the North China Basin, has been associated with ~N-S right-lateral strike-slip faulting (e.g., Ren et al., 2002).

A right-lateral shear zone running north over 2000 km from the eastern Japan Sea margin up to northern Sakhalin island guided the opening of the Japan and Okhotsk seas during the Oligo-Miocene (Figure 1a; Lallemand and Jolivet, 1985; Jolivet and Huchon, 1989; Jolivet et al., 1991, 1992; Jolivet and Tamaki, 1992; Tamaki et al., 1992; Fournier et al., 1994, 1995). Jolivet et al. (1991) estimated the amount of motion along the shear zone at ~400 km during the opening of the Japan Sea. Jolivet et al. (1992) and Fournier et al. (1994) showed that the deformation along the shear zone evolved from transtensional near the subduction zone to transpressional in the northern continental part. This led them to relate extension to subduction and strike-slip faulting to continental deformation, i.e., India-Asia collision. Kimura and Tamaki (1986), putting forward the geometry of the deformation in Asia, and Jolivet et al. (1990), interpreting the laboratory experiments of Davy and Cobbold (1988), had already related the opening of the Japan Sea to the India-Asia collision.

The current opening of the Okinawa Trough is dominated by oblique rifting and N-S dextral shear. The main grabens within the trough are arranged with a dextral en-echelon pattern and are associated with N-S rigth-lateral strike-slip faults (Eguchi and Uyeda, 1983; Sibuet et al., 1987; Imanishi et al., 1996; Fournier et al., 2001).

Dextral shear has also been recognised along the East Vietnam margin during the opening of the South China Sea in the Oligo-Miocene. Several studies have evidenced that the Indochina peninsula was strongly deformed at that time between the dextral shear zone which bounds the Indian indenter to the west and the East Vietnam fault (Marquis et al., 1997, Roques et al., 1997). Contemporaneous extension south of the Red River Ailao Shan shear zone (Bukhang dome) and in the Song Hong basin allowed Jolivet et al. (1999) to propose a dextral bookshelf model for the deformation of Indochina during the opening of the South China Sea.

In northern China, Nabelek et al. (1987) and Chen and Nabelek (1988) showed that active normal faulting and subsidence in the North China Basin are linked with dextral strike-slip faulting along the East Taihang, Cang Xian-Dongning, and Tan-Lu fault systems. They proposed that the North China Basin opened as a pull-apart basin along the right-lateral Tan-Lu fault system (Lu et al., 1983, Xu et al., 1987), which was confirmed by the structural and stratigraphic study of the Bohai basin (Allen et al., 1997).

1.3. Change of boundary conditions in Middle Miocene

The collisions of the Australian and Philippine Sea plates with the south-eastern and eastern Asian margins started in the Late-Early and Middle Miocene (e.g., Hall, 1996, 2002). In Sulawesi, the Sula and Buton blocks, headlands of the Australian plate, collided first with the north Sulawesi island arc, south easternmost extension of the Asian margin (Hamilton, 1979, Silver et al., 1983b, Rangin et al., 1990). An intra-oceanic subduction was subsequently initiated to the south. At the same time, convergence and shortening started in SE Asia with the inception of the south-eastward subductions of the Proto South China Sea and the Sulu basin in the Palawan and south Sulu Sea trenches, respectively (Holloway, 1982, Rangin et al., 1990). The subduction of the South China Sea, Sulu and Celebes marginal basins in the Manilla, Negros, and Cotobato trenches started in the Late-Middle Miocene (Maleterre, 1989). During the Pliocene, the collision zone was duplicated to the south, in Timor, where the northern Australian margin started to collide with the Banda arc (Audley- Charles, 1981, Milsom and Audley-Charles, 1986, Charlton et al., 1991, Harris, 1991). The deformation front progressed northward and, on the northern edge of the Banda arc, the southward subduction of the Banda Sea basin was initiated along the Flores and Wetar thrusts (Silver et al., 1983b). At the same time, the Borneo and Sunda shelf basins experienced a major inversion, which started during Miocene time some 17 Ma ago (Daly et al., 1991). Sundaland

presently behaves as a rigid plate and its motion is controlled by the subduction of the Indian plate in the Java trench (Chamot-Rooke and Le Pichon, 1999).

Island arcs carried by the Philippine Sea Plate started to collide with the eastern Asian margin in Middle Miocene, first the Bonin arc in central Japan (Itoh, 1988) followed by the Luzon arc in Taiwan 5 Ma ago (Ho, 1986). In Japan, the onset of the present-day compressional regime was recorded between 10 Ma and 7 Ma (Jolivet and Tamaki, 1992; Tamaki et al., 1992). Compression perpendicular to the trenches is documented by dike and fault set measurements (Nakamura and Uyeda, 1980; Yamagishi and Watanabe, 1986; Jolivet and Huchon, 1989; Jolivet et al., 1991), earthquake focal mechanisms (e.g., Yamazaki et al., 1985; Fukao and Furumoto, 1975), and geodetic measurements (Heki et al., 1990; Mazzotti et al., 2000, 2001; Henri et al., 2001). The later data shows a strong coupling between the Japan arc and the Pacific plate. Crustal shortening is also taken up by thrust faulting in the northern part of the Philippine Sea Plate (Zenisu ridge) (Chamot-Rooke and Pichon, 1989; Lallemant et al., 1989). In Taiwan, collision began during the Pliocene and the present-day convergence rate measured by GPS amounts 86 mm/yr along N307°E (Yu and Chen, 1994). Convergence results in crustal shortening taken up by active thrust faults in the Longitudinal Valley and at the western thrust front.

Collisions of Australia and Philippine Sea plates with the Asian margins in Middle Miocene time ultimately resulted in the present-day compression generalized to all the boundaries of Asia, except above the Ryukyu trench where the Okinawa Trough opens. They might have stopped the opening of marginal basins and led to closure. In contrast, landward, northern China has been little affected by the changes of stress regime along the subduction zone and still undergoes strike-slip and normal faulting. Sakhalin has also been preserved from the change of boundary conditions and it is still dominated by strike-slip and reverse faulting, as in Miocene time (Fournier et al., 1994; Areviev et al., 2000).

1.4. Conclusion

The recent pattern of deformation shows a strong coupling between the Asian (s.l.) lithosphere and the subducting plates in Japan as well as in Indonesia, whereas before the Middle (SE Asia) or Late Miocene (Japan) the eastern and south-eastern Asian margins were streched and deformed by extension. The existence of dextral shear zones along the eastern margin of Asia interacting with marginal extension in the Japan Sea region (Lallemand and Jolivet, 1985; Jolivet et al., 1990; 1994) has been generalized to the whole margin of Asia from the northernmost Okhotsk Sea (Fournier et al., 1994; Worrall et al., 1996), the north China grabens (Chen and Nabelek, 1988), the Ryukyu region (Fournier et al., 2001), to the western margin of the South China Sea (Marquis et al., 1997, Roques et al., 1997). Continental deformation would be responsible through strike-slip faulting for the geometry of opening of the basins, and the component of extension required for the opening would be provided by the subduction.

Tapponnier and Molnar (1976) and Tapponnier et al. (1982) first proposed that the south and east Asian boundaries acted as stress-free boundaries during the collision of India and that continental blocks were extruded toward the east. This hypothesis, relying on the asymmetry of the deformation pattern in Asia, is partly corroborated by recent GPS measurements: one fourth to one third of the India-Eurasia convergence is currently transferred to the eastward extrusion of continental blocks (Figure 1b; Molnar and Gipson, 1996; Heki et al., 1999; Larson et al., 1999; Shen et al., 2000; Wang et al., 2001). Several experiments of analogue and numerical modelling of continental deformation were performed with passive free boundaries (Tapponnier et al., 1982; Vilotte et al., 1982; Vilotte et al., 1984; Cohen and Morgan, 1986; Vilotte et al., 1986; Davy and Cobbold, 1988; Peltzer and Tapponnier, 1988; Houseman and England, 1993). So far, the influence of dynamic marginal

extension upon continental deformation in context of collision had not been tested by means of models. We performed laboratory experiments of indentation by a rigid indenter of a model of lithosphere subject to gravitational spreading to understand how collision and extension can interact in continental deformation, and how a drastic change of boundary conditions may have an influence on deformation inside the continent.

2. Experimental process

Modelling continental deformation requires to choose suitable boundary conditions and to define the fundamental behaviour of deforming continental lithosphere. The main difference between the analogue experiments and the numerical models lies in the response of the lithosphere to stress. In laboratory experiments, the rheological structure of the deformed media generally favours the brittle behaviour (Coulomb's law of friction) by allowing the localisation of the deformation in plasticine (Tapponnier et al., 1982; Peltzer and Tapponnier, 1988) or in sand layers (Davy and Cobbold, 1988, 1991; Davy et al., 1995). On the opposite, numerical models assume that the lithosphere can be described as a continuum, local discontinuities being averaged over a scale of about 50-100 km (Vilotte et al., 1982, 1986; Houseman and England, 1986; 1993; Cohen and Morgan, 1986). This assumption deserves a careful testing since faults exist up to several thousand kilometres. As a consequence, tectonic maps cannot be directly compared to numerical models.

In their experiments, Tapponnier et al. (1982) and Peltzer and Tapponnier (1988) imposed a plane strain condition (no thickening) which inevitably resulted in lateral expulsion of rigid blocks sliding past one another along localized zones of deformation. More recent analogue and numerical models (Cohen and Morgan, 1986; Houseman and England, 1986; Vilotte et al., 1986; Davy and Cobbold, 1988, 1991; Houseman and England, 1993, 1996; Kong and Bird, 1996; England and Molnar, 1997; Flesch et al., 2001) included buoyancy

forces, which means that the models thickened in reasonable proportions and thinned when the deviatoric stress exceeded the shear strength. The works of England and Molnar (1997) and Flesch et al. (2001) confirm the strong influence of the gravitational potential energy differences on the strain field. Houseman and England (1993, 1996) described numerical experiments with a model including buoyancy forces and with a lithostatic eastern boundary. The deviatoric stress was zero along the boundary which was allowed to move under the influence of indentation only. Consequently, there was little extension along the eastern margin of the model. Davy and Cobbold (1988) performed analogue experiments with a weakly confined eastern boundary. The deviatoric stress was not zero along the boundary, but the model did not spread because the deviatoric stress was lower than the shear strength of the model. In the first part of this paper, we stated the importance of extensional deformation along the south-eastern and eastern boundaries of Asia during the first part of the collision. In continuity with the work of Davy and Cobbold (1988), we attempted to characterise the role of extension during indentation. We built a model of continental lithosphere with a gravity potential higher than its integrated shear strength, so that it could spread under its own weight provided that boundary conditions permitted it. With this type of weak unstable lithospere model, the deformation pattern is more diffuse than for a strong plate. The distribution and the amount of extension in the experiments are therefore not similar to the natural case. Consequently, the experiments can not be quantitatively compared to the natural examples, but they bring qualitative information about the deformation produced by collision-indentation on an extending plate.

2.1. Rheological properties of the model

We used a rheological model of continental lithosphere made of 3 layers resting upon an asthenosphere of glucose syrup (Davy and Cobbold, 1991). The physical parameters for

each experiment and the scaling values are given in Table 1 and 2, respectively. The upper crust is assumed to be brittle with a Mohr-Coulomb frictional behaviour (Byerlee, 1968). It is modelled with dry quartz sand, which obeys a frictional sliding Mohr-Coulomb criterion with a negligible cohesion and a frictional angle of ~30°. The lower crust and the upper mantle are modelled with two Newtonian silicone putties of different viscosities and densities, the upper mantle having higher viscosity and density than the lower crust. The silicone putty is a nearly Newtonian fluid which obeys a creep law where deviatoric stress linearly increases with strain rate. The glucose syrup is a Newtonian fluid of low viscosity (10-100 Pa s) and high density (~1400 kg m^{-3}). Further discussion and justification of the experimental method can be found in Davy and Cobbold (1991) and in Faccenna et al. (1999).

2.2. Boundary conditions

The southern (lower) boundary of the model was strained by a rigid indenter progressing northward (Figure 2 and Table 1). The northern (upper) and western (lateral left) boundaries of the model were in contact with the rigid experimental box. The eastern (lateral right) and southeastern (lower right) boundaries were “free”, i.e., the lithosphere model was at isostatic equilibrium directly with the asthenosphere (glucose syrup). In two experiments, the eastern boundary was weakly confined with a five millimetre thick silicone putty layer floating on glucose syrup. This increased the gravity potential of the boundary and slowed down lateral spreading of the model. However, whether it was free or weakly confined, the eastern boundary always allowed lateral spreading of the model.

2.3. Scaling for gravitational spreading

The experiments were scaled for the normal gravitational field given the physical properties of materials and setting the thickness of a normal crust, about 30 km in nature, to

1.5 cm in the experiments (Table 2). The initial dimensions of the model are shown in Figure 2. Under the latter conditions, the width of the model (75 cm) represented 1500 km, its length (95 cm) represented 1900 km, and the width of the indenter (35 cm) represented 700 km which is about one third of the distance between the two Indian syntaxes. Because of its large dimensions, the model was uneasy to build and manipulate and it was not conceivable to build a larger model.

In the experiments, two forces compete in the process of gravitational spreading. The differential hydrostatic pressure between the lithosphere and the asthenosphere favours gravitational collapse of the lithosphere, and the integrated shear strength of the model prevents it. Spreading occurs when the gravity potential of the model with respect to the free boundary exceeds the integrated shear strength of the lithosphere. The ratio between the potential energy difference and the total resistance of the lithosphere corresponds to the Argand number of England and McKenzie (1982; see also Faccenna et al., 1999). The Argand number can be approximated for the experiments in neglecting the shear strength of the silicone putty with respect to that of the sand. The integrated shear strength of the lithosphere becomes a function of the thickness of the sand layer only. The strength of the brittle layer is calculated using the frictional sliding criterion of Ranalli (1995; $\sigma_1-\sigma_3 = (R-1)\rho gh$; where R is a constant proportional to the coefficient of friction of the sand, which is ~0.5, and ρ and h are the density and thickness of the sand layer, respectively). The gravity potential of the model relative to the boundary depends on the thickness of the (brittle and ductile) crust only, as the density of the lithospheric mantle is similar to that of the asthenosphere in the experiments. With these approximations, the Argand number of the experiments is nearly constant and between 3 and 4. These calculations were confirmed by experimental tests, which showed that spreading occurred as soon as the ductile crust was thicker than the brittle crust. We chose a

thickness of 0.5 cm for the brittle crust and 1 cm for the ductile crust, i.e., 10 km and 20 km in nature, respectively (Tables 1 and 2).

Time scales characteristic of deformations produced by indentation and gravitational spreading have been evaluated. We performed preliminary tests to measure spreading rates in the absence of indentation. The free boundary of a 30 cm large model of lithosphere advanced at a rate of 1 to 2 $cm.h^{-1}$ (depending on whether the boundary was weakly confined or totally free, respectively), which corresponds to a strain rate of 1 to 2.10^{-5} s^{-1} calculated along a line perpendicular to the free boundary. The strain rate produced by indentation calculated along a line perpendicular to the indenter was between 2 and 6.10^{-5} s^{-1}, depending on the speed of the indenter which varied between 6 and 20 $cm.h^{-1}$ (Table 1). Thus, the time scales characteristic of indentation and gravitational spreading in the experiments were of the same order of magnitude, the two phenomenon could interact and be compared to each other.

2.4. Testing different boundary conditions

Three parameters were tested during the experiments: the duration of extension, the extension rate, and the indentation velocity. The duration of extension and the extension rate control the amount of finite extension.

The duration of extension corresponds to the duration of the experiment. In the first experiment (E1 thereafter), we let the model spread one hour before beginning the indentation. During the initial stage of spreading, homogeneously distributed normal faults appeared in the model. These faults were reactivated during the second part of the experiment under the effect of indentation. In the other experiments (E2, E3, and E4 thereafter), no initial spreading occurred before indentation (Table 1).

The extension rate was controlled by modifying the gravity potential of the model with respect to the eastern boundary, with the presence or the absence of a lateral confinement. The

eastern boundary was confined with a five millimetre thick silicone layer in E1 and E2 (Table 1), which increased the gravity potential of the boundary and reduced the spreading rate of the model. In E3 and E4, we removed the confinement and the gravity potential of the model was increased.

The three first experiments were performed with an almost constant indentation velocity between 5.5 and 7 $cm.h^{-1}$ (Table 1). We increased the indenter velocity to 20 $cm.h^{-1}$ for E4.

2.5. Method of strain analysis

To record the deformation, the models were covered by an orthogonal grid made of white sand lines spaced every two centimetres. The deformation of the grid was monitored by photography every 15 minutes. The grids of the initial and final stages have been digitised from enlarged photographs. The error margin on the location of the grid nodes is less than 1 mm in the N-S and E-W directions. The finite displacement field with respect to the experimental box is given by the initial and final positions of the grid nodes. A structural map of the final stage of each experiment has been drawn from the photographs.

We used continuum mechanics to analyse the deformation. In continuum mechanics, a finite homogeneous strain is described by the deformation gradient tensor (F) which gives the relationship between a vector joining two points at the initial and the final stage. F can be decomposed in an antisymmetric matrix which describes a rotation, called rotation tensor (R), and a symmetric matrix which can be related to the strain ellipse (in 2D) and which correspond to the usual geological meaning of finite strain, often called stretch tensor (e.g., Jaeger and Cook, 1979; McKenzie and Jackson, 1983). Because matrix multiplication is not in general commutative, there are two ways of making this decomposition depending on whether the rotation is carried out before or after the finite strain:

$F = RU$ or $F = VR$

where U is the right stretch tensor and V is the left stretch tensor. U and V have the same eigenvalues, which are the principal strains (principal axes of the strain ellipse), but their eigenvectors are different and correspond to the orientation of the principal axes before deformation in the case of U, and after deformation in the case of V. The finite strain ellipse after deformation, which gives a picture of the local strain, is obtained from V and the surface dilatation, which corresponds to the ratio of the change in area to the original surface, is given by the determinant of U, V, or F. The rotation of the principal strain axes between their initial and final states is calculated from R. Finally, we found in the large literature concerned with continuum mechanics a strain tensor known as Almansi-Euler strain tensor (E) and defined as:

$E = 1/2 (I - V^{-2})$

where I is the unit matrix (Salençon, 1995). The determinant of the Almansi-Euler strain tensor proved to be an excellent indicator of the strike-slip faults in the experiments, that we called "shear factor" (the determinant of the Almansi-Euler strain tensor is also a good indicator of isotropic contraction, which does not occur in the experiments). It is given between 0 and 1 in non-dimensional units. Thus, a complete set of strain parameters has been obtained to be analysed and compared to the deformation of Asia.

3. Experimental results

3.1. Common pattern of deformation

The structural evolution was similar for all the experiments. Experiment 2 (E2) is shown as an example in Figure 3. Folds and thrust faults first appeared in front of the indenter. After 90 to 120 minutes of indentation at ~6 $cm.h^{-1}$, a wide left-lateral shear zone trending SW-NE was individualised joining the folded zone to the NE corner of the model. It was associated with antithetic right-lateral shear zones starting from the eastern edge of the

indenter, more or less developed depending on boundary conditions (Figure 3b). In the southeastern part of the model, grabens formed in a large extensional domain exempt from strike-slip fault. Some grabens opened as extrado cracks perpendicular to the curvature of the eastern and southern boundaries. Afterwards, the compression zone in front of the indenter widened. It encompassed a triangular zone preserved from deformation and bounded to the north by en échelon folds and thrusts. In the NE part of the model, antithetic right-lateral shear zones appeared in the left-lateral deformation zone. They bound rigid blocks which rotated counterclockwise. Grabens opened at the southern extremities of these right-lateral shear zones (Figure 3c). At this stage, the deformation pattern was definitively settled. It was asymmetric because the eastern free boundary favoured the development of a major left-lateral deformation zone, which accommodated eastward extrusion.

An analysis of the deformation is shown in Figures 4 to 7 for the experiments E1 to E4, respectively, with (a) a structural map at the final stage of the experiment, (b) the finite displacement field relative to the experimental box, and (c) a map of the finite strain ellipse. Figure 8 shows (a) a map of the shear factor, (b) a map of rotation of the principal strain axes, and (c) a map of surface dilatation (changes in surface area) for each experiment.

3.2. Diffuse versus localized deformation

The structural maps and the shear factor maps bring complementary information about the degree of localization of the deformation in the experiments. The shear factor maps show whether the deformation is homogeneous or if it is localized along major faults. The shear factor is maximum near the two edges of the indenter and is always larger on left side of the indenter, near the fixed wall of the experimental box, than on the right side near the free boundary (Figure 8a). The shear factor decreases with the distance to the indenter, as the convergence is partly taken up by shortening. In the absence of lateral confinement (E3 and

E4) , the deformation is diffuse and accommodated by a dense network of conjugate strike-slip faults (Figures 6a, 7a, and 8a). The conjugate faults are distributed almost symmetrically over a triangular deformation zone heading toward the northeast. When the eastern boundary is confined (E1 and E2), the deformation is localized along a few major strike-slip faults (Figures 4a, 5a, and 8a). A system of conjugate strike-slip faults appears in front of the indenter. It encompasses a prominent left-lateral shear zone trending SW-NE, associated with less developed N-S right-lateral faults starting from the eastern edge of the indenter. Another system of minor conjugate shear zones also appears to the northeast of the unstrained triangle in E1 (Figures 4a and 8a).

In case of preliminary spreading before indentation (E1), the left-lateral strike-slip faults which appear during the indentation partly reactivate normal faults which formed during the preliminary spreading. During the preliminary extension, normal faults were distributed all over the model except in the northwestern corner, with a SW-NE mean trend perpendicular to the direction of spreading. The northwesternmost normal faults were curved toward the northwest. In E1, the left-lateral strike-slip faults, which appeared when the indentation began, reactivated these northwestern curved normal faults (Figures 4a and 8a). That is the reason why the deformation pattern in E1 is shifted toward the north in comparison with E2 (Figures 5a and 8a). Thus, in E1 the localization of the deformation occurred after an initial stage of diffuse extension.

3.3. Kinematics of finite deformation

Figures 4b, 5b, 6b, and 7b show the finite displacement fields relative to the experimental box for each experiment. The displacements are approximately circular about a fixed point with respect to the experimental box, whose position depends on the boundary conditions. The fixed point can be compared to an Euler rotation pole which describes the

motion of the main part of the model (except the northwestern corner) with respect to the experimental box, although the deformation is distributed and the model does not behave as a rigid plate. When the eastern boundary is confined (E1 and E2), the fixed point is located immediately east of the indenter (Figures 4b and 5b). The lateral confinement favours extrusion and spreading toward the southern free boundary and the formation of a "return flow" on the right of the indenter. The mean direction of the "return flow" changes from ~N-S in E1 to NW-SE in E2, because of the preliminary stage of spreading in E1 which highly contributes to the southward component of the "return flow". Vilotte et al. (1982) obtained a similar displacement field in case of plane strain with a rigid lateral boundary. In the absence of lateral confinement (E3 and E4), extrusion and spreading toward the eastern boundary are favoured and the fixed point is located more eastward (Figure 6b and 7b). In E3, a substantial "return flow" appeared to the east of the indenter, whereas in E4 the displacement field is centered on the SE corner of the model because the high indentation velocity (20 $cm.h^{-1}$) and the low duration of the experiment (1 h 30 mn) prevented southward motions. Similar velocity fields have been obtained in numerical and analogue experiments in case of plain strain with a free lateral boundary (Vilotte et al., 1982; Peltzer and Tapponnier, 1988), and the gravitational spreading does not modify significantly this velocity field. Thus, the position of the fixed point mainly depends on the boundary conditions: lateral confinement favours southward escape and brings the fixed point close to the indenter.

The maps of displacement field and shear rate show that the main structure which controls the kinematics of the deformation is the NE trending left-lateral shear zone (Figures 4b, 4b, 6b, 7b, and 8a). It transforms the northward motion of indentation in eastward extrusion. A component of gravitational spreading toward the free boundaries is added to the component of "rigid" extrusion (see section 3.4). The N-S right-lateral fault zones which developed in E1 and E2 from the eastern edge of the indenter have little influence on the

displacement field, though they are well defined on the shear rate maps and accommodated displacements of the centimetre scale in the experiments (Figures 4a, 5a, and 8a). These displacements are negligible with respect to the eastward displacements. This shows that the choice of faults is of crucial importance in the calculation of displacement field from rates of motion along faults, which already requires a strong hypothesis on the mechanism of deformation.

3.4. Rigid extrusion and gravitational spreading

Rigid extrusion can be discriminated from gravitational spreading in the experiments in studying the variations of the eastward component of the velocity along lines originally E-W. Extrusion is defined as the part of the N-S convergence (indentation) which is transferred in lateral motions by the strike-slip faults, the other part being taken up by shortening in front of the indenter. Figure 9a shows the eastward velocity relative to the experimental box versus the distance from the western wall of the experimental box, for each experiment. Velocities have been averaged over a 10 cm large originally E-W stripe of the central part of the model (i.e., over six E-W lines spaced every two centimetres located between 40 and 50 cm from the southern boundary). The velocity curves in Figure 9a have a sigmoidal shape and can be divided in three parts corresponding to zones to the west, to the north, and to the east of the indenter. The velocity increases first slowly to the west of the indenter, then quickly to the north of the indenter, and again slowly to the east of the indenter. Figure 9b gives a simple interpretation of these curves. The eastward velocity can be considered as the sum of rigid extrusion and gravitational spreading. In the absence of indentation, the component of gravitational spreading increases linearly from west to east since the silicone putty has a Newtonian behaviour (when the model is thickened by indentation, the gravitational potential of the model increases with the topographic load in front of the indenter, and the spreading

velocity increases; however, this effect is negligible in the experimental curves of Figure 9a because the velocities have been measured beyond the thickened zone). During indentation, the eastward velocity increases north of the indenter, as the northward indentation motion is transferred in eastward motion by the left-lateral strike-slip faults. East of the indenter, the eastward velocity increases slowly due to gravitational spreading only. The extrusion velocity can be determined from the experimental curves with a linear extrapolation of the gravitational spreading velocity east of the indenter (Figure 9 and Table 3).

The velocity of gravitational spreading depends on the eastern boundary condition (Table 2): it is between 2.8 ±0.8 and 3.6 ±0.6 $cm.h^{-1}$ when the eastern boundary is free (E3 and E4) and between 0.4 ±0.5 and 0.8 ±0.5 $cm.h^{-1}$ when the boundary is weakly confined (E1 and E2). The extrusion velocity is about one half of the indentation velocity : it is between 2.5 ±0.4 $cm.h^{-1}$ and 3.6 ±0.3 $cm.h^{-1}$ when the indentation velocity is ~6 $cm.h^{-1}$ (E1, E2, and E3), and it is 11.4 ±0.6$cm.h^{-1}$ when the indentation velocity is 20 ±0.3 $cm.h^{-1}$ (E4). If the shortening velocity is the indentation velocity minus the extrusion velocity, the shortening/extrusion ratio is about 1 (between 0.8 and 1.8) for the four experiments (Table 3).

3.5. Rotations about vertical axes

The rotations are maximum (>50°) near the two edges of the indenter where the shear rate is maximum (Figures 8b). The rotation maps are asymmetric with a prominent NE trending stripe of counterclockwise (CCW) rotations corresponding to the major left-lateral deformation zone, and clockwise (CW) rotations in the SE part of the model. In the left-lateral shear zone, the CCW rotations reach 20-25° in E1, E2, and E3, and 30° in E4, when the amount of shortening is maximum. In the SE part of the model, the CW rotations exceed 30° in all the experiments. When the deformation is localised (E1 and E2), the stripe of CCW rotations is disrupted by one or several ~N-S narrow stripes of CW rotations which

correspond to conjugate right-lateral shear zones (Figure 8b). When the deformation is diffuse (E3 and E4), no CW rotation associated with right-lateral shear zone can be individualised (Figure 8b).

In the SE part of the model, the pattern of CW rotation depends on the boundary conditions. When the eastern boundary is free (E3 and E4), the southeastern part of the model rotates clockwise freely during indentation and the rotation rates increase southward (Figure 8b). Similar observations were made by Tapponnier et al. (1982), Vilotte et al. (1984), and Davy and Cobbold (1988) with models with a lateral free boundary. When the eastern boundary is confined (E1 and E2), the model is almost attached to the eastern wall of the experimental box and cannot rotate freely during indentation. The rotations are low along the eastern boundary. The N-S right-lateral shear between the indenter and the eastern boundary is taken up locally on the eastern edge of the indenter. Figure 3c of the final stage of E2 shows that the originally E-W lines are dextrally sheared on the eastern edge of the indenter and remain ~E-W near the eastern boundary.

The rotation maps illustrate that rotations can be related either to shear along fault zones, or to rotation of large blocks together with faults. They also show that lateral confinement acts upon the deformation of the SE part of the model by preventing the free rotation of the model: indentation is accommodated by global rotation of the SE part of the model in the absence of lateral confinement, and by N-S shear to the east of the indenter when the eastern boundary is confined, which isolates the southeastern part of the model from the indentation zone.

3.6. Change in area and topography

The surface dilatation (change in area) is expressed as the ratio of the final area of the strain ellipse to its initial area, in percent (Figure 8c). The change in surface area corresponds

to change in volume during strain, i.e., to change in thickness of the lithosphere model. Hence, they also correspond to variations in topography since the model is at isostatic equilibrium. A decrease in area is equivalent to an elevation of topography, and an increase in area is equivalent to a fall in topography.

Thickening is limited in the experiments because it is quickly compensated by gravitational spreading. Thickening is higher when the indentation velocity is higher (E4; Figure 8c), or when there is no initial spreading and the eastern boundary is confined (E2; Figure 8c). The maps show the asymmetric pattern of the thickened lithosphere in front of the indenter. Thickening is more important to the west, near the fixed wall of the experimental box, than to the east near the free boundary. Thickening is localised ahead of the indenter and in the southern part of the NE trending left-lateral deformation zone (Figure 8c). The asymmetric distribution of thickened lithosphere is related to the existence of the left-lateral deformation zone, which localises part of the thickening.

3.7. Driving forces of deformation and opening of marginal basins

The deformation in the experiments is driven by two processes: (1) collision which produces thickening accommodated by folding and thrust faulting, and lateral extrusion accommodated by strike-slip faulting, and (2) gravitational spreading which produces thinning accommodated by normal faulting. Yet, it is not easy to discriminate in the finite strain the part related to collision and the part related to gravitational spreading. Following Ramsay (1967), three strain fields have been distinguished on the maps of the finite strain ellipse (Figures 4c, 5c, 6c, and 7c). The field of contraction (in grey) corresponds to strain characterised by two shortened principal axes (or quadratic elongation values lower than 1), and the field of dilatation (in white) corresponds to strain characterised by two lengthened principal axes (or quadratic elongation values greater than 1). The intermediate strain field, or

field of compensation (in black), is reserved for strain with the least strain axis shortened and the greatest strain axis lengthened.

In the experiments, the NW part of the model is indifferently in the compensation, dilatation, or contraction field, because little deformation occurs in this area.

The SE part of the model is always in the field of dilatation, which implies that the deformation is driven by gravitational spreading. This part of the model is translated eastward and rotates clockwise under the effect of the indentation, but the influence of indentation upon its internal strain is negligible. The grabens are perpendicular to the direction of spreading: E-W when the east boundary is confined and spreading mainly directed toward the south (E1 and E2; Figures 4a and 5a), and NW-SE or NE-SW when the east and south boundary are free (flattening prevails) (E3 and E4; Figures 6a and 7a).

The NE part of the model is mainly in the compensation field and partly in the dilatation field. It is the place where indentation and gravitational spreading interacts and where basins form along strike-slip faults. Figure 10 show a detailed structural map of this area for E2. NE-SW left-lateral shear in the main deformation zone is accommodated by CCW rotation of rigid blocks bounded by NNW trending right-lateral strike-slip faults. The blocks rotate 10 to 25° counterclockwise and the rotation may exceed 10° clockwise in the right-lateral fault zones (Figure 8b). Grabens form as pull-apart basins between the right-lateral strike-slip faults or as tension fractures at the southern extremity of the strike-slip faults. The grabens geometry is entirely controlled by the conjugate strike-slip faults produced by indentation.

3.8. Conclusion

The deformation pattern in the experiments is mainly controlled by the gravity potential of the model. The deformation is localised when the gravity potential is limited by

confinement of the eastern boundary (E1 and E2), even if indentation has been preceded by preliminary spreading (E1). The deformation is diffuse when the eastern boundary is free and the gravity potential is higher (E3 and E4). The indentation velocity has little influence on the deformation pattern.

The finite displacement field relative to the experimental box is roughly circular about a fixed point located to the east of the indenter. This fixed point moves eastward when lateral confinement is removed. The major structure which controls the kinematics of deformation is the NE-trending left-lateral deformation zone.

The rotations are related to shear along faults except in the southeastern part of the model which rotates freely in the absence of lateral confinement. When the eastern boundary is confined, the northward motion of the indenter is accommodated by a huge N-S dextral shear zone on the eastern edge of the indenter.

The graben formation is linked with strike-slip faulting related to indentation in the NE part of the model, and it is driven by gravity only in the SE part.

4. Comparison with the deformation of the Asian lithosphere

As previously stated, extension is overestimated in the experiments and the results cannot be quantitatively compared to the deformation of Asia. However, they bring qualitative information about the way indentation and extension interact and how boundary conditions have an influence upon the deformation far inside the continent.

4.1. Current and finite kinematics of Asia

The present-day velocity field in Asia is roughly circular around the eastern Indian syntaxis (Figure 1b; Molnar and Lyon-Caen, 1989; Avouac and Tapponnier, 1993; Holt et al., 1995; Peltzer and Saucier, 1996; Larson et al., 1999; Holt et al., 2000), which validates a

posteriori the hypothesis of Tapponnier and Molnar (1976) of a free boundary along the eastern Asian margin. East of longitude 100°E, the southeastern and eastern Asia including Sundaland, South China, North China, and the Amurian plate moves eastward at a mean rate of ~1 cm/yr relative to stable Eurasia (Molnar and Gibson, 1996; Chamot-Rooke and Le Pichon, 1999; Heki et al., 1999; Larson et al., 1999; Shen et al., 2000; Wang et al., 2001). The relative motions between the main continental blocks of eastern Asia are low (of the order of few mm/yr), and a wide region extending from the Baikal Rift to the Japan Sea and to SE Asia and Indonesia is slowly extruded eastward. The present-day velocity field in Asia is thus characterised by an extrusion toward the east, no "return flow", and a rotation pole to the southeast of the eastern Indian Syntaxis. Because of the absence of "return flow", this velocity field would rather correspond to an experiment with a free boundary to the east, that is E3 or E4.

The finite kinematics of Asia since the Eocene is poorly constrained because it is unclear to what extent extrusion took part in the finite deformation and because the boundary conditions of Asia were different in the Oligo-Miocene. Attempts at reconstruction of the finite displacement field have been realised assuming that Asia is a mosaic of rigid crustal blocks bounded by faults (Cobbold and Davy, 1988; Replumaz, 1999). These reconstructions rely mainly on the extrapolation over large periods of the current velocity field and Quaternary fault slip rates, and the error margins remain important. Nevertheless, the directions of relative motion in southeast Asia are fairly well constrained for the Oligo-Miocene period. The strike-slip motions along the Red River Fault and the eastern coast of South Vietnam can be described with a rotation pole located east of the Indian indenter (8°N, 86°E; Leloup et al., 1995, 2001, Harrison et al., 1996; Marquis et al., 1997; Roques et al., 1997), which also corresponds to the opening pole of the South China Sea (Briais et al., 1993). This pole, which accounts for the main relative motions in southeast Asia during the

32-17 Ma period, is near the eastern Indian syntaxis. If this Euler pole could be assimilated to the fixed point of the experiments, it would rather correspond to an experiment with a confined boundary to the east, that is E1 and E2.

Paleomagnetism provides a complementary approach of the finite kinematics of Asia, independent from fault patterns and slip rates. Paleomagnetic studies of Cretaceous formations allowed to propose reconstructions of central Asia prior to the collision of India, in which the total amount of N-S convergence between India and Asia is distributed within the Asian plate (Chen et al., 1993; Halim et al., 1998). Halim et al. (1998) showed that the convergence between the northern Asian blocks and stable Siberia was too large to have been taken up by shortening only in the Tien Shan and Altay mountain ranges. They concluded that the Pamir-Okhotsk deformation zone played a major role during the collision and accommodated several hundreds kilometres of left-lateral strike-slip motions between deforming Asia and the Siberian platform. Evidences for left-lateral motions have been described along this deformation zone. From Tien Shan to Altai, the en échelon arrangement of the mountain ranges suggests left-lateral shear (Argand, 1922; Cobbold and Davy, 1988; Thomas et al., 2002). In the Baikal region, normal slip prevails on NE-trending fault planes, associated with left-lateral slip along E-W strike-slip faults (Tapponnier and Molnar, 1979, Hutchinson et al., 1992, Deverchère et al., 1993). In the Stanovoy ranges, left-lateral slip is evidenced along active E-W strike-slip faults by earthquake focal mechanisms (Parfenoy et al., 1987). Worrall et al. (1996) showed that the left-lateral deformation extended to the northernmost part of the Sea of Okhotsk and the Bering Strait through a series of NE-SW trending grabens associated with E-W left-lateral faults zones. This major left-lateral deformation zone, which cut Asia from Pamir to the Okhotsk Sea, is still currently active (Figure 1b). It is equivalent to the NE trending left-lateral deformation zone which appears in all the laboratory experiments when the eastern boundary is free.

4.2. Rotations in southeast Asia

Clockwise rotations have been widely documented by paleomagnetism in Cretaceous formations of southeast Asia (Achache et al., 1983; Otofuji et al., 1990; Funahara et al., 1992; 1993; Huang and Opdyke, 1993; Chen et al., 1993; Halim et al., 1998). It has been demonstrated that some of these rotations occurred during the Paleocene (Funahara et al., 1992). Paleomagnetic data do not show that southeast Asia rotated as a single coherent unit in response to the India-Asia collision, but suggests that most of the rotations occurred before the onset of the collisions of the Australian and Philippine Sea plates with the Asian margins in Middle Miocene time. This situation can be compared to the experiments E3 and E4 with an east free boundary. When the model is not attached to the experimental box, the southeastern part of the model rotated freely during indentation (Figure 11a).

On the opposite, Cobbold and Davy (1988) and England and Molnar (1990) pointed out that the present-day deformation of the eastern margin of Tibet is dominated by large left-lateral active strike-slip faults which separate blocks that are rotating clockwise in a huge N-S right-lateral shear zone (Dewey et al., 1988; Huang et al., 1992). This shear zone allows the northward motion of Tibet relative to South China to be taken up locally on the eastern margin of the Tibetan plateau. This situation corresponds to the experiments E1 and E2 with an east confined boundary: the southeastern part of the model is linked to the experimental box and the N-S right-lateral shear due to the northward motion of the indenter is taken up on the eastern edge of the indenter (Figure 11b).

As suggested in Figure 11, the change of boundary conditions in eastern Asia in Middle Miocene time with the collisions of the Australian and Philippines Sea plates, may have precluded the rotation of SE Asia and provoked a large-scale change in the way the deformation is accommodated far from the subduction zones.

4.3. Opening of marginal basins

As stated in the first part, the geometry of back arc basins in eastern Asia is controlled by ~N-S dextral strike-slip faults (Fournier, 1994). In the Okhotsk Sea and North China Basins areas, the dextral Sakhalin-Hokkaido and Tanlu fault systems intersect with the conjugate and coeval sinistral Baikal-Stanovoy and Qinling fault systems, which pertain to the sinistral faults system extending from the Pamir zone to the Okhotsk Sea which accommodated the extrusion tectonics of Asia (Figure 1a). The large-scale deformation pattern of Asia strongly suggests that the effects of the India-Eurasia collision extended at least as far northeastward as the Okhotsk Sea. The close similarity of the first-order deformation pattern of Asia to small-scale analog models (Davy and Cobbold, 1988) led Jolivet et al. (1990) to propose a model of opening of the NE Asian basins (Japan sea and North China Basin) in relation with the India-Eurasia collision. In this model, the convergence between India and Asia is partly taken up along a wide left-lateral shear zone which connects the Pamir to the Stanovoy ranges and evolves from transpression to transtension (Figure 1a). In the transtensional domain, left-lateral shear is accommodated by rotation of large crustal blocks bounded by right-lateral strike-slip zones, the east Japan Sea shear zone, the Tan-Lu Fault, and en echelon grabens on rims of the Ordos block. Worrall et al. (1996) extended this model up to the Kamchatka and the Bering Strait. The experiment E2 lends additional support to this interpretation, and even shows that left-lateral shear can be totally taken up by counterclockwise rotations and right-lateral shear in the absence of major left-lateral shear zones.

In southeast Asia several back arc basins (South China Sea, Celebes and Sulu basins) opened during the Tertiary. It has been proposed that the opening of the South China Sea was related to the India-Eurasia collision (Tapponnier et al., 1982, 1986). In the experiments, no

major shear zone interacts with the extensional domain to the SE, which forms only as a consequence of gravitational spreading. According to the experiments, back arc basins in the north would thus be pull-apart basins controlled by dextral shear zones and basins in SE Asia would be classical back arc basins with no interference with collision effects.

4.4. Asymmetric topography distribution in Asia

The distribution of the topography in Asia is asymmetric with respect to the ~N-S direction of India-Asia convergence (Figure 1b). Topography exceeds 1000 m throughout a triangular area heading NE toward the Stanovoy ranges from the Himalayan arc. Higher topographies above 4000 m are found in Himalayas, Tibet, and Pamir, i.e., in front of the Indian indenter, and along the NW margin of the topography triangle which is marked by a series of mountain ranges including from SW to NE the Hindu Kush, the northern Pamir, the Tien Shan and the Altai. These mountain ranges belong to the Pamir-Baikal-Okhotsk left-lateral deformation zone. The same topography distribution is observed in the experiments. A triangular thickened zone heading toward the NE is observed in E4 (Figure 8c) when the indentation velocity is several times higher than the spreading velocity. In E1 and E2 (Figure 8c), a thickened zone is observed in the southwestern part of the major NE trending left-lateral shear zone.

Conclusion

We investigated the role of extension driven by gravity during continental deformation produced by collision, by means of analogue models. The experiments provide a model for the opening of the major marginal basins and continental grabens of eastern Asia related to right-lateral strike-slip faulting, in the framework of the India-Asia collision and the marginal extension above the retreating slabs of the western Pacific. Several origins have so far been

proposed for the extensional deformation in Asia: subduction along the eastern and south-eastern boundaries, collision with India and consecutive deformation of Asia, mantle plume under the Baikal region, and gravitational spreading in Tibet. In case of subduction and mantle plume, the high heat flow generated at the base of the crust tend to decrease the integrated shear strength of the crust. This possibly makes it spread toward regions of low stress, e.g., subduction zones. If so, extension along subduction zones and above mantle plumes is driven by gravity, as in regions where the crust is thickened. We do not take into account thermal phenomenons in the experiments. Gravity is used to produce extensional deformation along the boundaries of the model. As discussed above, this experimental assumption is not necessarily unrealistic. The experiments show that gravity and collision-related deformation interact in the NE part of the model, as continental deformation and subduction-related extension interacted in NE Asia during the opening of the main basins. Because of the chosen rheology, the models do not show any rigid extrusion of a block that could be compared to Indochina. However, the experiments suggest that the opening of marginal basins in SE Asia is more likely the result of subduction-related extension only.

Our experiments bring a physical basis to models which put the emphasis on a large-scale left-lateral shear zone running from the western Indian syntaxis to the Okhotsk Sea, to N-S trending dextral shear zones which control the geometry of backarc basins, and to distributed extension in SE Asia controlled solely by slab retreat. Whether extension is further enhanced by the thermal structure of the lithosphere (e.g., hot regions, Miyashiro, 1986) is open to discussion.

Acknowledgments. The experiments were performed in the tectonic experimental laboratory of Rennes with the technical assistance of J. J. Kermarrec. We thank T. Nalpas and J.-M.

Daniel for their help during the experiments and in computing the deformation grids, and Evgenii Burov and Hugues Raimbourg for scientific discussions during the review process. The manuscript greatly benefited from the reviews of Claudio Faccenna and Lucy Flesch. Figures were drafted using GMT software (Wessel and Smith, 1991).

References

Achache, J., V. Courtillot, and J. Besse, Paleomagnetic constraints on the late Cretaceous and Cenozoic tectonics of southeastern Asia, Earth Planet. Sci. Lett., **63**, 123-136, 1983.

Allen, M. B., D. I. M. Macdonald, S. J. Vincent, X. Zhao, and C. Brouet-Menzies, Early Cenozoic two-phase extension and late Cenozoic thermal subsidence and inversion of the Bohai Basin, northern China, Mar. Pet. Geol., **14**, 951-972, 1997.

Argand, E., La tectonique de l'Asie, Congrès géologique International, XIII Session, Belgique, 171-372, 1922.

Argus, D. F., and R. G. Gordon, No-net-rotation model of current plate velocities incorporating plate motion model NUVEL-1, *Geophys. Res. Lett.*, **18**, 2039-2042, 1991.

Arefiev, S., E. Rogozhin, R. Tatevossian, L. Rivera and A. Cisternas, The Neftegorsk (Sakhalin Island) 1995 earthquake: a rare interplate event, *Geophys. J. Int.*, **143**, 595-608, 2000.

Armijo, R., P. Tapponnier, J. L. Mercier and H. Tonglin, Quaternary extension in southern Tibet: field observations and tectonic implications, *J. Geophys. Res.*, **91**, 13,803-13,872, 1986.

Armijo, R., P. Tapponnier and H. Tonglin, Late Cenozoic right-lateral strike-slip faulting in southern Tibet, *J. Geophys. Res.*, **94**, 2787-2838, 1989.

Audley-Charles, M. G., Geometrical problems and implications of large scale overthrusting in the Banda Arc-Australian margin collision zone, *Spec. Publ. Geol. Soc. Lon.,* **9,** 407-416, 1981.

Avouac, J. P. and P. Tapponnier, Kinematic model of active deformation in central Asia, *Geophys. Res. Lett.,* **20**, 895-898, 1993.

Bellier, O., J. Mercier, P. Vergely, C. Long and C Ning, Evolution sédimentaire et tectonique du graben Mésozoique de la Wei He (province du Shanxi, Chine du Nord), *Bull. Soc. geol. France*, **4**, 979-994, 1988.

Bird, P., Lateral extrusion of lower crust from under high topography in the isostatic limit, *J. Geophys. Res.*, **96**, 10275-10286, 1991.

Briais, A., P. Patriat and P. Tapponnier, Updated interpretation of magnetic anomalies and seafloor spreading stages in the South China Sea: implications for the tertiary tectonics of SE Asia, *J. Geophys. Res.*, **98**, 6229-6328, 1993.

Burchfiel, B. C. and L. H. Royden, North-south extension within the convergent Himalayan region, *Geology*, **13**, 679-682, 1985.

Burchfiel, B. C. and L. H. Royden, Tectonics of Asia 50 years after the death of Emile Argand, *Eclogae Geol. Helv.,* **84**, 599-629, 1991.

Burchfiel, B. C., C. Zhiliang, K. V. Hodges, L. Yuping, L. H. Royden, D. Changrong and X. Jiene, The south Tibetan detachment system, Himalayan orogen: extension comtemporaneous with and parallel to shortening in a collisional mountain belt, *Geol. Soc. Amer. Spec. Pap.,* **269**, 1-41, 1992.

Burg, J. P., M. Guiraud, G. M. Chen and G. C. Li, Himalayan metamorphism and deformations in the North Himalayan Belt (southern Tibet, China), *Earth Planet. Sci. Lett.,* **69**, 391-400, 1984.

Byerlee, J. D., Brittle-ductile transition in rocks, J. Geophys. Res., 73, 4741-4750, 1968.

Chamot-Rooke, N. and X. L. Pichon, Zenisu ridge: Mechanical model of formation, *Tectonophysics*, **160**, 175-194, 1989.

Chamot-Rooke N., and X. Le Pichon, GPS determined eastward Sundaland motion with respect to Eurasia confirmed by earthquakes slip vectors at Sunda and Philippine trenches, *Earth Planet. Sci. Lett.,* **173**, 439-455, 1999.

Charlton, T. R., A. J. Barber and S. T. Barkham, The structural evolution of the Timor collision complex, eastern Indonesia, *J. Struct. Geol.,* **13**, 489-500, 1991.

Chen, Y., V. Courtillot, J. P. Cogné, J. Besse, Z. Yang, and R.J. Enkin, The configuration of Asia prior to the collision of India: Cretaceous paleomagnetic constraints, *J. Geophys. Res.,* **98**, 21,927-21,941, 1993.

Chen, W. P. and J. Nabelek, Seismogenic strike-slip faulting and the development of the North China basin, *Tectonics*, **7**, 975-989, 1988.

Cobbold, P. R. and P. Davy, Indentation tectonics in nature and experiments. 2. Central Asia, *Bulletin of the Geological institutions of Upsalla*, **14**, 143-162, 1988.

Cohen, S. C. and R. C. Morgan, Intraplate deformation due to continental collisions: a numerical study of deformation in a thin viscous sheet, *Tectonophysics*, **132**, 247-259, 1986.

Coleman, M. and K. Hodges, Evidence for Tibetan Plateau uplift before 14 Myr ago from a new minmum age for east-west extension, *Nature*, **374**, 49-52, 1995.

Crétaux, J.-F., L. Soudarin, A. Cazenave, and F. Bouillé, Present-day tectonic plate motions and crustal deformations from the DORIS space system, *J. Geophys. Res.*, **103**, 30,167-30,181, 1998.

Daly, M. C., M. A. Cooper, I. Wilson, D. G. Smith and B. G. D. Hooper, Cenozoic plate tectonics and basin evolution in Indonesia, *Mar. Petrol. Geol.,* **8**, 2-21, 1991.

Davy, P. and P. R. Cobbold, Indentation tectonics in nature and experiments. Experiments scaled for gravity, *Bulletin of the Geological Institutions of Upsalla*, **14**, 129-141, 1988.

Davy, P. and P. R. Cobbold, Experiments on shortening of a 4-layer model of the continental lithosphere, *Tectonophysics*, **188**, 1-25, 1991.

Davy, P., A. Hansen, E. Bonnet, and S. -Z. Zhang, Localization and fault growth in layered brittle-ductile systems: Implications for deformations of the continental lithosphere, *J. Geophys. Res.,* **100**, 6281-6294, 1995

DeMets, C., R.G. Gordon, D.F. Argus, S. Stein, Current plate motion, *Geophys. J. Int.,* **101**, 425-478, 1990.

DeMets, C., R.G. Gordon, D.F. Argus, S. Stein, Effects of recent revisions to the geomagnetic reversal time scale on estimates of current plates motions, *Geophys. Res. Lett.*, **21**, 2191-2194, 1994.

Deverchère, J., F. Houdry, N. V. Solonenko, A. V. Solonenko and V. A. Sankov, Seismicity, active faults and stress field of the north Muya region, Baikal rift: new insights on the rheology of extende continental lithosphere, *J. Geophys. Res.*, **98**, 19,895-19,912, 1993.

Dewey, J. F., S. Cande and W. C. I. Pitman, Tectonic evolution of the India-Eurasia collision zone, *Eclogae geol. Helv.*, **82**, 717-734, 1989.

Dewey, J. F., R. M. Shackleton, Chang Chengfa, and Sun Yiyin, The tectonic evolution of the Tibetan plateau, Phil. Trans. R. Soc. Lond., A 327, 379-413, 1988.

Eguchi, T., and S. Uyeda, Seismotectonics of the Okinawa trough and Ryukyu arc, *Mem. Geol. Soc. China,* **5**, 189-210, 1983.

Engdahl, E.R., R. van der Hilst, and R. Buland, Global teleseismic earthquake relocation with improved travel times and procedures for depth determination, *Bull. Seismol. Soc. Am.,* **88**, 722-743, 1998.

England, P., G. A. Houseman, and L. Sonder, Length scales for continental deformation in convergent, divergent, and strike-slip environments: Analytical and approximate solutions for a thin viscous sheet model, *J. Geophys. Res.*, **90**, 523-532, 1985.

England, P. and G. A. Houseman, Finite strain calculations of continental deformation. II: application to the India-Asia collision, *J. Geophys. Res.*, **91**, 3664-3676, 1986.

England, P. and D. P. McKenzie, A thin viscous sheet model for continental deformation, *Geophys. J. R. Astron. Soc.,* **70**, 295-321, 1982.

England, P. and P. Molnar, Right-lateral shear and rotation as the explanation for strike-slip faulting in eastern Tibet, *Nature*, **344**, 140-142, 1990.

England, P. and P. Molnar, The field of crustal velocity in Asia calculated from Quaternary rates of slip on faults, *Geophys. J. Int.,* **130**, 551-582, 1997.

Faccenna, C., P. Davy, J.P. Brun, R. Funiciello, D. Giardini, M. Mattei, and T. Nalpas, The dynamics of back-arc extensions: A laboratory approach to the opening of the Tyrrhenian Sea, *Geophys. J. Int.,* **126**, 781-795, 1996.

Faccenna, C., D. Giardini, P. Davy, and A. Argentieri, Initiation of subduction at Atlantic-type margins: Insights from laboratory experiments, *J. Geophys. Res.,* **104**, 2749-2766, 1999.

Flesch, L. M., A. J. Haines, ans W. E. Holt, Dynamics of the India-Eurasia collision zone, J. Geophys. Res., 106 , 16,435-16,460, 2001.

Fournier, M., Ouverture de bassins marginaux et déformation continentale : L'exemple de la mer du Japon, PhD Thesis, University Paris 6, 312 pp., 1994.

Fournier, M., L. Jolivet, P. Huchon, V. S. Rozhdestvensky, K. F. Sergeyev and L. Oscorbin, Neogene strike-slip faulting in Sakhalin, and the Japan Sea opening, J. Geophys. Res., **99**, 2701-2725, 1994.

Fournier, M., L. Jolivet, and O. Fabbri, Neogene stress field in SW Japan and mechanism of deformation during the Japan Sea opening, *J. Geophys. Res.*, **100**, 24,295-24,314, 1995.

Fournier, M., O. Fabbri, J. Angelier, and J.P. Cadet, Kinematics and timing of opening of the Okinawa Trough: Insights from regional seismicity and onland deformation in the Ryukyu arc, *J. Geophys. Res.*, **106**, 13,751-13768, 2001.

Fukao, Y. and M. Furumoto, Mechanisms of large earthquakes along the eastern margin of the Japan Sea, *Tectonophysics*, **25**, 247-266, 1975.

Funahara, S., N. Nishiwaki, M. Miki, F. Muruta, Y. Otofuji, and Yi Zhao Wang, Paleomagnetic study of Cretaceous rocks from the Yangtze block, central Yunnan, China: implications for the India-Asia collision, *Earth Planet. Sci. Lett.,* **113**, 77-91, 1992.

Funahara, S., N. Nishiwaki, F. Muruta, Y. Otofuji, and Yi Zhao Wang, Clockwise rotation of the Red River fault inferred from paleomagnetic study of Cretaceous rocks in the Shan-Thai-Malay block of western Yunnan, China, *Earth Planet. Sci. Lett.,* **117**, 29-42, 1993.

Halim, N., J. P. Cogné, Y. Chen, R. Atasiei, J. Besse, V. Courtillot, S. Gilder, J. Marcoux, and R. L. Zhao, New Cretaceous and Early Tertiary paleomagnetic results from Xining-Lanzhou basin, Kunlun and Qiangtang blocks, China: Implications on the geodynamic evolution of Asia, *J. Geophys. Res.,* **103**, 21,025-21,045, 1998.

Hall, R., Reconstructing Cenozoic SE Asia, in Tectonic Evolution of Southeast Asia, edited by R. Hall and D. Blundell, *Geol. Soc. Spec. Pub.,* **106**, 153-184, 1996.

Hall, R., Cenozoic geological and plate tectonic evolution of SE Asia and the SW Pacific: computer-based reconstructions, model and animations, *J. Asian Earth Sci.,* **20**, 353-43, 2002.

Hamilton, W., Tectonics of the Indonesian region, U.S. Geological Survey Prof. Pap., 1078, 345 p., 1979.

Harris, R. A., Temporal distribution of strain in the active Banda orogen: a reconciliation of rival hypotheses, in Orogenis in action, Journal of southeast Asian earth science, edited by R. Hall, G. Nichols and C. Rangin, pp. 5, 1991.

Harrison, T.M., P. H. Leloup, F.J. Ryerson, P. Tapponnier, R. Lacassin, and W. Chen, Diachronous initiation of transtension along the Ailao San-Red River shear zone, Yunnan

and Vietnam, in *The Tectonic Evolution of Asia*, edited by A. Lin and T. M. Harrison, pp. 208-226, Cambridge University Press, New York, 1996.

Heki, K. Horizontal and vertical crustal movements from three-dimensional very long baseline interferometry kinematic reference frame: Implication for the reversal timescale revision, *J. Geophys. Res.,* **101**, 3187-3198, 1996.

Heki, K., Y. Takahashi and T. Kondo, Contraction of northeastern Japan: evidence from horizontal displacement of a Japanese station in global very long baseline interferometry networks, *Tectonophysics*, **181**, 113-122, 1990.

Heki, K., S. Miyazaki, H. Takahashi, M. Kasahara, F. Kimata, S. Miura, N. F. Vasilenko, A. Ivashchenko, and K.-D. An, The Amurian Plate motion and current plate kinematics in eastern Asia, *J. Geophys. Res.,* **104**, 29,147-29,155, 1999.

Hellinger, S. J., K. M. Shedloock, J. G. Sclater and Y. Hong, The Cenozoic evolution of the noth China basin, *Tectonics*, **4**, 343-358, 1985.

Henry, P., S. Mazzotti, and X. Le Pichon, Transient and permanent deformation of central Japan estimated by GPS - 1. Interseismic loading and subduction kinematics, *Earth Planet. Sci. Lett.,* **184**, 443-453, 2001.

Ho, C. S., A synthesis of the geologic evolution of Taiwan, *Tectonophysics*, 125, 1-16, 1986.

Holloway, N. H., The stratigraphy and tectonic relationship of Reed Bank, north Palawan and Mindoro to the Asian mainland and its significance in the evolution of the South China Sea, *Amer. Assoc. Petrol. Bull.,* **66**, 1357-1383, 1982.

Holt, E. H. and A. J. Haines, Velocity field in deforming Asia from the inversion of earthquake-released strains, *Tectonics*, **12**, 1-20, 1993.

Holt, E. H., M. Li, and A. J. Haines, Earthquake strain rates and instantaneous relative motion within central and east Asia, *Geophys. J. Int.,* **122**, 569-593, 1995.

Holt, E. H., J. F. Ni, T. C. Wallace and A. J. Haines, The active tectonics of the eastern Himalayan syntaxis and surrounding regions, *J. Geophys. Res.,* **96**, 14,595-14,632, 1991.

Holt, W. E., N. Chamot-Rooke, X. Le Pichon, A. J. Haines, B. Shen-Tu, and J. Ren, Velocity field in Asia inferred from Quaternary fault slip rates and Global Positioning System observations, *J. Geophys. Res.,* **105**, 19,185-19,209, 2000.

Hong, Y., K. M. Shedlock, S. J. Hellinger and J. G. Sclater, The North China Basin: an example of a Cenozoic rifted intraplate basin, *Tectonics*, **4**, 153-169, 1985.

Houseman, G. and P. England, Finite strain calculations of continental deformation. 1. Method and general results for convergent zones, *J. Geophys. Res.,* **91**, 3651-3663, 1986.

Houseman, G. and P. England, Crustal thickening versus lateral expulsion in the Indian-Asian continental collision, *J. Geophys. Res.,* **98**, 12,233-12,249, 1993.

Houseman, G. and P. England, A lithospheric-thickening model for the Indo-Asian collision, in *Tectonic Evolution of Asia*, Edited by A. Yin and T. M. Harrison, Cambridge Univ. Press, New York, 3-17, 1996.

Huang, K., N. D. Opdyke, J. Li, and X. Peng, Paleomagnetism of Cretaceous rocks from eastern Qiangtang terrane of eastern Tibet, *J. Geophys. Res.,* **97**, 1789-1799, 1992.

Huang, K., and N. D. Opdyke, Paleomagnetic results from Cretaceous and Jurassic rocks of south and southwest Yunnan: evidence for large clockwise rotations in the Indochina and Shan-Thai-Malay terranes, *Earth Planet. Sci. Lett.,* **117**, 507-524, 1993.

Hutchinson, D. R., A. J. Golmshtok, L. P. Zonenshain, T. C. Moore, C. A. Scholz and K. D. Klitgord, Depositional and tectonic framework of the rift basins of lake Baikal from multichannel seismic data, *Geology*, **20**, 589-592, 1992.

Imanishi, M., F. Kimata, N. Inamori, R. Miyajima, T. Okuda, K. Takai, K. Hirahara, and T. Kato, Horizontal displacements by GPS measurements at the Okinawa-Sakishima Islands (1994-1995), *J. Seismol. Soc. Jpn.,* **49**, 417-421, 1996.

Itoh, Y., Differential rotation of the eastern part of Southwest Japan inferred from paleomagnetism of Cretaceous and Neogene rocks, *J. Geophys. Res.*, 93, 3401-3411, 1988.

Jaeger and Cook, *Fundamentals of rocks mechanism*, Third Edition, Chapman and Hall, London, 1979.

Jolivet, L., P. Davy and P. Cobbold, Right-lateral shear along the northwest Pacific margin and the India-Eurasia collision, *Tectonics*, **9**, 1409-1419, 1990.

Jolivet, L., M. Fournier, P. Huchon, V. S. Rozhdestvenskiy, S. Sergeyev and L. S. Oscorbin, Cenozoic intracontinental dextral motion in the Okhotsk-Japan Sea region, *Tectonics*, **11**, 968-977, 1992.

Jolivet, L. and P. Huchon, Crustal scale strike-slip deformation in Hokkaido, Northeast Japan, *J. Struct. Geol.*, **11**, 509-522, 1989.

Jolivet, L., P. Huchon, J. P. Brun, N. Chamot-Rooke, X. Le Pichon and J. C. Thomas, Arc deformation and marginal basin opening, Japan Sea as a case study, *J. Geophys. Res.*, **96**, 4367-4384, 1991.

Jolivet, L., C. Lepvrier, H. Maluski, O. Beyssac, B. Goffé, Nguyen Van Vuong, and Phan Truong Thi, Oligocene-Miocene Bu Khang extensional gneiss dome in Vietnam: Geodynamic implications, *Geology*, **27**, 67–70, 1999.

Jolivet, L. and K. Tamaki, Neogene Kinematics in the Japan Sea region and the volcanic activity of the Northeast Japan arc, in *Proc. ODP, Sci. Results*, edited by K. Tamaki, K. Suyehiro, J. Allan, M. McWilliams and e. al., pp. 1311-1331, Ocean Drilling Program, College Station, TX, 1992.

Jolivet, L., K. Tamaki and M. Fournier, Japan Sea, opening history and mechanism, a synthesis, *J. Geophys. Res.*, **99**, 22237-22259, 1994.

Karig, D. E., Origin and development of marginal basins in the western Pacific, *J. Geophys. Res.*, **76**, 2542-2561, 1971.

Kimura, G. and K. Tamaki, Collision, rotation and back arc spreading: the case of the Okhotsk and Japan seas, *Tectonics*, **5**, 389-401, 1986.

Kong, X., and P. Bird, Neotectonics of Asia: Thin-shell finite-element models with faults, in *Tectonic Evolution of Asia*, Edited by A. Yin and T. M. Harrison, Cambridge Univ. Press, New York, 18-34, 1996.

Lallemand, S. and L. Jolivet, Japan Sea: a pull apart basin, *Earth Planet. Sci. Lett.*, **76**, 375-389, 1985.

Lallemant, S., N. Chamot-Rooke, X. Le Pichon and C. Rangin, Zenisu Ridge: A deep intra-oceanic thrust related to subduction off Southwest Japan, *Tectonophysics*, **160**, 151-174, 1989.

Larson, K. M., R. Bürgmann, R. Bilham, and J. T. Freymueller, Kinematics of the India-Eurasia collision zone from GPS measurements, *J. Geophys. Res.*, **104**, 1077-1093, 1999.

Leloup P.H., R. Lacassin, P. Tapponnier, U. Schärer, Zhong D., Liu X., Zhang L., Ji S. and T. Phan Trong, The Ailao Shan-Red River shear zone (Yunnan, China), Tertiary transform boundary of Indochina, *Tectonophysics*, **251**, 3-84, 1995.

Leloup, P. H., N. Arnaud, R. Lacassin, J. R. Kienast, T. M. Harrison, T. T. Phan Trong, A. Replumaz, and P. Tapponnier, New constraints on the structure, thermochronology, and timing of the Ailao Shan-Red River shear zone, SE Asia, *J. Geophys. Res.*, **106**, 6683-6732, 2001.

Le Pichon, X., Land-locked ocean basin and continental collision in the eastern Mediterranean area as a case example, in Mountain building process, edited by K. J. Hsu, pp. 201-213, Academic, San Diego, California, 1982.

Le Pichon, X., M. Fournier and L. Jolivet, Kinematics, topography, shortening and extrusion in the India-Eurasia collision, Tectonics, **11**, 1085-1098, 1992.

Lu, H., H. Yu, Y. Ding and Q. Zhang, Changing stress field in the middle segment of the Tan-Lu fault zone, eastern China, *Tectonophysics*, **98**, 253-270, 1983.

Ma, X. and D. Wu, Cenozoic extensional tectonics in China, *Tectonophysics*, **133**, 243-255, 1987.

Maleterre, P., Histoire sédimentaire, magmatique, tectonique et métallogénique d'un arc cénozoique déformé en régime de transpression, Univ. Bretagne Occidentale, Thèse de doctorat, 304 p., 1989.

Marquis, G., D. Roques, P. Huchon, O. Coulon, N. Chamot-Rooke, C. Rangin and X. Le Pichon, Amount and timing of extension along the continental margin off central Vietnam, *Bull. Soc. Géol. France*, **168**, 707-716, 1997.

Martinod, J., and P. Davy, Periodic instabilities during compression of the lithosphere, 2, Analogue experiments, *J. Geophys. Res.*, **99**, 12,057-12,069, 1994.

Mazzotti, S., P. Henry, X. Le Pichon and T. Sagiya, Strain partitioning in the zone of transition from Nankai subduction to Izu-Bonin collision (Central Japan): implications for an extensional tear within the subducting slab, *Earth Planet. Sci. Lett.*, **172**, 1-10, 1999.

Mazzotti, S., P. Henry and X. Le Pichon, Transient and permanent deformation of central Japan estimated by GPS - 2. Strain partitioning and arc-arc collision, *Earth Planet. Sci. Lett.*, **184**, 455-469, 2001.

McKenzie, D. P., Speculations on the consequences and causes of plate motions, *Geophys. J. Roy. Astron. Soc.*, **18**, 1-32, 1969.

McKenzie, D. P., and J. Jackson, The relationship between strain rates, crustal thickening, paleomagnetism, finite strain and fault movements within a deforming zone, *Earth Planet. Sci. Lett.*, **65**, 182-202, 1983.

Mercier, J. L., R. Armijo, P. Tapponnier, E. Carey-Gailhardis and H. T. Lin, Change from Late Tertiary compression to Quaternary extension in southern Tibet during the India-Asia collision, *Tectonics*, **6**, 275-304, 1987.

Milsom, J. and M. R. Audley-Charles, Post collisional isostatic adjustment in the southern Banda arc, in Collision Tectonics, *Spec. Publ. Geol. Soc. Lon.,* edited by pp. 353-366, 1986.

Miyashiro, A., Hot regions and the origin of marginal basins in the western Pacific, *Tectonophysics*, **122**, 195-216, 1986.

Molnar, P. and T. Atwater, Interarc spreading and cordilleran tectonics as alternates related to the age of the subducted oceanic lithosphere, *Earth Planet. Sci. Lett.*, **41**, 330-340, 1978.

Molnar, P., B. C. Burchfield, L. K'uangyi and Z. Ziyun, Geomorphic evidence for active faulting in the Altyn Tagh and northern Tibet and qualitative estimates of its contribution to the convergence of India and Eurasia, *Geology*, **15**, 249-253, 1987.

Molnar, P., and Deng Quidong, Faulting associated with large earthquakes and the average rate of deformation in central and eastern Asia, *J. Geophys. Res.*, **89**, 6203-6227, 1984.

Molnar, P.; and J. M. Gipson, A bound on the rheology of continental lithosphere using very long baseline interferometry: The velocity of south China with respect to Eurasia, *J. Geophys. Res.*, **101**, 545-554, 1996.

Molnar, P. and W. P. Chen, Focal depths and fault plane solutions of earthquakes under the Tibetan plateau, *J. Geophys. Res.*, **88**, 1180-1196, 1983.

Molnar, P., and H. Lyon-Caen, Fault plane solutions of earthquakes and active tectonics of the Tibetan plateau and its margins, *Geophys. J. Int.*, **99**, 123-153, 1989.

Molnar, P. and P. Tapponnier, Cenozoic tectonics of Asia: Effects of a continental collision, *Science*, **189**, 419-426, 1975.

Molnar, P. and P. Tapponnier, Active tectonics of Tibet, *J. Geophys. Res.*, **83**, 5361-5375, 1978.

Nabelek, J., W. P. Chen and H. Ye, The Tangshan earthquake sequence of 1976 and its implications for the evolution of the North China basin, *J. Geophys. Res.*, **92**, 12615-12628, 1987.

Nakamura, K. and S. Uyeda, Stress gradient in back arc regions and plate subduction, *J. Geophys. Res.*, **85**, 6419-6428, 1980.

Otofuji, Y., Y. Inoue, S. Funahara, F. Murata, and X. Zheng, Paleomagnetic study of eastern Tibet-deformation of the Three Rivers region, *Geophys. J. Int.*, **103**, 85-94, 1990.

Pan, Y. and W. S. F. Kidd, Nyainqentanghla shear zone: a late Miocene extensional detachment in the southern Tibetan plateau, *Geology*, **20**, 775-778, 1992.

Peltzer, G., and F. Saucier, Present-day kinematics of Asia derived from geologic fault rates, *J. Geophys. Res.*, **101**, 27,943-27,956, 1996.

Peltzer, G. and P. Tapponnier, Formation and evolution of strike-slip faults, rifts and basins during the India-Asia collision: an experimental approach, *J. Geophys. Res.*, **93**, 15085-15118, 1988.

Qin, C., C. Papazachos, and E. Papadimitriou, Velocity field for crustal deformation in China derived from seismic moment tensor summation of earthquakes, *Tectonophysics,* **359**, 29-46, 2002.

Ramsay, J. G., Folding and fracturing of rocks, McGraw-Hill Book Company, New-York, 560 p., 1967.

Ranalli, G., Rheology of the Earth, pp. 1-413, Chapman and Hall, New York, 1995.

Rangin, C., L. Jolivet, M. Pubellier et al., A simple model for the tectonic evolution of southeast Asia and Indonesia region for the past 43 Ma, *Bull. Soc. Géol. France*, **6**, 889-906, 1990.

Ren, J., K. Tamaki, Sitian Li and Zhang Junxia, Late Mesozoic and Cenozoic rifting and its dynamic setting in Eastern China and adjacent areas, *Tectonophysics*, **344**, 175-205, 2002.

Replumaz, A., Reconstruction de la zone de collision Inde-Asie: Etude centrée sur l'Indochine, Ph. D. Thesis, 229 pp., Univ. Paris 7, Paris, 1999.

Roques, D., C. Rangin and P. Huchon, Geometry and sense of motion along the Vietnam continental margin: onshore/offshore Da Nang area, *Bull. Soc. Géol. France*, **168**, 413-422, 1997.

Salençon, J., Mécanique du continu, Tome 1, Concepts généraux, Ed. Ellipse, Paris, pp. 352, 1995.

Shemenda, A. I., and A. L. Grokholski, Physical modelling of lithosphere in collision zones, *Tectonophysics*, **216**, 273-290, 1992.

Shen, Z.-K., C. Zhao, A. Yin, Y. Li, D. D. Jackson, P. Fang, and D. Dong, Contemporary crustal deformation in east Asia constrained by Global Positioning System measurements, *J. Geophys. Res.*, **105**, 5721-5734, 2000.

Sibuet, J. C., J. Letouzey, F. Barbier, J. Charvet, J. P. Foucher, T. W. C. Hilde, M. Kimura, C. Lin-Yun, B. Marsset, C. Muller and J. F. Stephan, Back-arc extension in the Okinawa trough, *J. Geophys. Res.*, **92**, 14041-14063, 1987.

Sibuet, J.C., S.-K. Hsu, C.T. Shyu, and C.S. Liu, Structural and kinematic evolutions of the Okinawa Trough backarc basin, in *Backarc Basins: Tectonics and Magmatism*, edited by B. Taylor, pp. 343-379, Plenum, New York, 1995.

Sibuet, J.C., B. Deffontaines, S.-K. Hsu, N. Thareau, J.P. Le Formal, C.S. Liu, and ACT party, Okinawa trough backarc basin: Early tectonic and magmatic evolution, *J. Geophys. Res.*, **103**, 30,245-30,267, 1998.

Silver, E. A., R. McCaffrey and R. B. Smith, Collision, rotation, and the initiation of subduction in the evolution of the Sulawesi, Indonesia, *J. Geophys. Res.*, **88**, 9407-9418, 1983a.

Silver, E. A. and C. Rangin, Developement of the Celebes Sea basin in the context of Western Pacific marginal basins history, in *Proc. ODP, Sci. Results*, edited by E. A. Silver, C. Rangin, M. T. Breymann and e. al., pp. 39-50, Ocean Drilling Program, College Station, TX, 1991a.

Silver, E. A. and C. Rangin, Leg 124 tectonic synthesis, in *Proc. ODP, Sci. Results*, edited by E. A. Silver, C. Rangin, M. T. Breymann and e. al., pp. 3-10, Ocean Drilling Program, College Station, TX, 1991b.

Silver, E. A., D. Reed, R. McCaffrey and Y. Joyodiwiryo, Back arc thrusting in the eastern Sunda arc, Indonesia: a consequence of arc-continent collision, *J. Geophys. Res.*, **88**, 7429-7448, 1983b.

Tamaki, K., Geological structure of the Japan sea and its tectonic implications, *Bulletin of the Geological Survey of Japan*, **39**, 269-365, 1988.

Tamaki, K., K. Suyehiro, J. Allan, J. C. Ingle and K. Pisciotto, Tectonic synthesis and implications of Japan Sea ODP drilling, in *Proc. ODP, Sci. Results*, edited by pp. 1333-1350, Ocean Drilling Program, College Station, TX, 1992.

Tapponnier, P., J. L. Mercier, R. Armijo, T. Han and J. Zhou, Field evidences for active normal faulting in Tibet, *Geology*, **294**, 410-414, 1981.

Tapponnier, P. and P. Molnar, Slip line field theory and large-scale continental tectonics, *Geology*, **264**, 319-324, 1976.

Tapponnier, P. and P. Molnar, Active faulting and Cenozoic tectonic of the Tien Shan, Mongolia, and Baykal regions, *J. Geophys. Res.*, **84**, 3425-3459, 1979.

Tapponnier, P., G. Peltzer and R. Armijo, On the mechanics of the collision between India and Asia, in *Collision tectonics*, *Geol. Soc. Spec. Pub.*, edited by M. P. Coward and A. C. Ries, pp. 115-157, 1986.

Tapponnier, P., G. Peltzer, A. Y. L. Dain, R. Armijo and P. Cobbold, Propagating extrusion tectonics in Asia: new insights from simple experiments with plasticine, *Geology*, **10**, 611-616, 1982.

Tatsumi, Y., Y. I. Otofuji, T. Matsuda and S. Nohda, Opening of the Sea of Japan back-arc basin by asthenospheric injection, *Tectonophysics*, **166**, 317-329, 1989.

Taylor, B. and D. E. Hayes, The tectonic evolution of the south China basin, in The tectonic and geologic evolution of southeast Asian seas and islands, *Geophys. Monogr.,* edited by D. E. Hayes, pp. 89-104, AGU, Washington, 1980.

Tian, Z., P. Hang and K. D. Xu, The Mesozoic-Cenozoic east China rift system, *Tectonophysics*, **208**, 341-363, 1992.

Thomas J. C., R. Lanza, A. Kazansky, V. Zykin, N. Semakov, D. Mitrokhin and D. Delvaux, Paleomagnetic study of Cenozoic sediments from the Zaisan basin (SE Kazakhstan) and the Chuya depression (Siberian Altai): tectonic implications for central Asia, Tectonophysics, 351, 119-137, 2002.

Uyeda, S. and H. Kanamori, Backarc opening and the mode of subduction, *J. Geophys. Res.*, **84**, 1049-106, 1979.

Vilotte, J. P., M. Daignières and R. Madariaga, Numerical modeling of intraplate deformation: simple mechanical models of continental collision, *J. Geophys. Res.*, **87**, 10,709-10,728, 1982.

Vilotte, J. P., M. Daignieres, R. Madariaga and O. C. Zienkiewicz, The role of a heteogeneous inclusion during continental collision, *Phys. Earth Planet. Int.,* **36**, 236-259, 1984.

Vilotte, J. P., R. Madariaga, M. Daignieres and O. C. Zienkiewicz, Numerical study of continental collision: influence of buoyancy forces and an initial stiff inclusion, *Geophys. J. R. Astr. Soc.,* **84**, 279-310, 1986.

Wang, J. M., The Fenwei rift and its recent periodic activity, *Tectonophysics*, **133**, 257-275, 1987.

Wang, Q., P.-Z. Zhang, J. T. Freymueller, R. Bilham, K. M. Larson, X. Lai, X. You, Z. Niu, J. Wu, Y. Li, J. Liu, Z. Yang, and Q. Chen, Present-day crustal deformation in China constrained by global positioning system measurements, *Science*, **294**, 574-577, 2001.

Weissel, J. K., Evidence for Eocene oceanic crust in the Celebes basin, in The tectonic and geologic evolution of southeast Asian seas and islands, *Geophys. Monogr.,* edited by H. D. E., pp. 37-47, AGU, Washington, 1980.

Wessel, P., and W. M. F. Smith, Free software helps map and display data, EOS Trans. AGU **72**, 441-446, 1991.

Windley, B. F. and M. B. Allen, Mongolian plateau: evidence for a late Cenozoic mantle plume under central Asia, *Geology*, **21**, 295-298, 1993.

Worrall, D. M., V. Kruglyak, F. Kunst and V. Kusnetsov, Tertiary tectonics of the Sea of Okhotsk, Russia: far-field effects of the India-Asia collision, *Tectonics,* **15**, 813-826, 1996.

Yu, S. B., and H. Y. Chen, Global positioning system measurements of crustal deformation in the Taiwan arc-continent collision zone, *Mem. Geol. Soc. China*, **5**, 477-498, 1994.

Xu, J., G. Zhu, W. X. Tong, K. R. Cui and Q. Liu, Formation and evolution of the Tancheng - Lujiang whrench fault sytem to the northwest of the Pacific ocean, *Tectonophysics*, **134**, 273-310, 1987.

Xu, X. and X. Ma, Geodynamics of the Shanxi rift system, *Tectonophysics*, **208**, 325-340, 1992.

Yamagishi, H. and Y. Watanabe, Change of stress field in Late Cenozoic, Southwest Hokkaido, Japan, - investigation of geologic faults, dykes, ore veins and active faults, *Monograph Geol. Collabor. Jpn.*, **31**, 321-332, 1986.

Yamazaki, K., T. Tamura and I Kawasaki, Seismogenic stress field of the Japan Sea as derived from shallow and small earthquakes, *J. Seismol. Soc. Japan*, **38**, 541-558, 1985.

FIGURE CAPTIONS

Figure 1. Deformation maps of Asia. (a) Tectonic map of Asia. AB is Aleutian Basin, AL is Altai range, AM is Amur plate, AS is Andaman Sea, ATF is Altyn Tagh Fault, BB is Bohai Basin, BK is Baikal rift, BS is Bering Sea, CS is Celebes Sea, FT is Flores Thrust, HB is Hetao Basins, JS is Japan Sea, KB is Kuril Basin, KF is Karakorum Fault, KJFZ is Karakorum-Jiali Fault Zone, KLF is Kunlun Fault, KYB is Komandorsky Basin, LMS is Longmen Shan, OB is Ordos block, OK is Okhotsk Sea, OT is Okinawa Trrough, PA is Pamir, QLS is Qinling Shan, RRF is Red River Fault, SB is Shanxi Basins, SCB is South China block, SCS is South China Sea, SF is Sagaing Fault, SLB is Shantar-Liziansky Basin, SS is Sulu Sea, STA is Stanovoy Range, SUF is Sumatra Fault, SUN is Sundaland, TB is Tarim block, TLF is Tan-Lu Fault, TPF is Tym-Poronaysk Fault, WB is Weihe Basin, WT is Wetar Thrust, XSF is Xanshuihe Fault, YB is Yinshuan Basins. (b) Topographic map of Asia, shallow seismicity (focal depth < 50 km; magnitude > 2) between 1964 and 1995 (Engdahl et al., 1998), and current GPS velocity field (Heflin et al., version 2002.3, http://sideshow.jpl.nasa.gov/mbh/series.html; Heki et al., 1999). with respect to the stable Eurasia plate in the NNR (no-net-rotation) NUVEL-1A plate motion model (DeMets et al., 1990; Argus and Gordon, 1991; DeMets et al., 1994).

Figure 2. Experimental device. The model of continental lithosphere made of 3 layers (sand, silicone 1, silicone 2) rests upon the asthenosphere made of glucose syrup. It is strained by a rigid indenter which progresses northward.

Figure 3. Successive deformation stages of E3.

Figure 4. Results of experiment E1. (a) Structural map at the final stage of the experiment. Continuous lines are fault traces, which are thrusts (triangle on hanging wall), strike-slip faults, or normal faults (ticks on hanging wall). Folds are continuous lines with arrow at both ends. (b) Finite displacement field relative to the experimental box. (c) Finite strain ellipse.

Figure 5. Results of experiment E2. Same legend as Figure 4. The successive stages of E2 are shown in Figure 3.

Figure 6. Results of experiment E3. Same legend as Figure 4.

Figure 7. Results of experiment E4. Same legend as Figure 4.

Figure 8. Results of experiments E1 to E4 : (a) "shear factor" (determinant of the Almansi-Euler stain tensor, see text), which is an indicator of strike-slip faults, (b) rotation in degree of the principal strain axes, and (c) surface dilatation, i.e., ratio of the change in area to the original surface.

Figure 9. (a) Curves of eastward velocity relative to the experimental box versus the distance from the western wall of the experimental box. (b) Interpretation: the eastward velocity is the sum of extrusion and gravitational spreading. V_{extr} is extrusion velocity.

Figure 10. Detailed structural map of the northeast part of the model for E3. Grabens form as pull-apart basins between right-lateral strike-slip faults or as tension fractures at the southern extremity of strike-slip faults.

Figure 11. Schematic evolution of the large-scale deformation and rotations in southeastern Asia with respect to boundary conditions. During the first part of the collision (Eocene to Early Miocene), the eastern Asian boundary was free and southeast Asia rotated freely. During the second part of the collision (Middle Miocene to Present), the rotation of southeast Asia was precluded by the collisions of the Australian and Philippines Sea plates and the northward motion of Tibet relative to South China was taken up locally on the eastern margin of the Tibetan plateau.

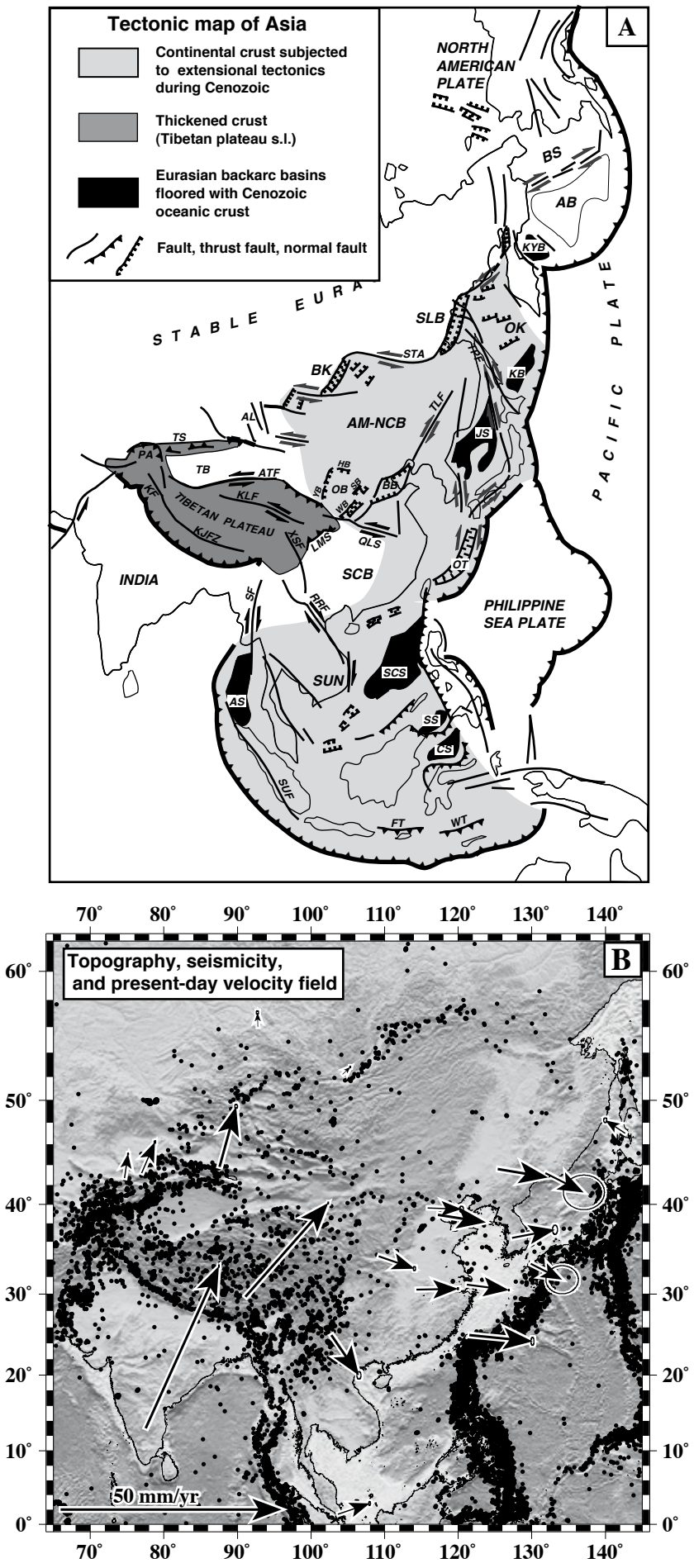
Tectonic map of Asia
Continental crust subjected to extensional tectonics during Cenozoic
Thickened crust (Tibetan plateau s.l.)
Eurasian backarc basins floored with Cenozoic oceanic crust
Fault, thrust fault, normal fault
A
NORTH AMERICAN PLATE
BS
AB
KYB
STABLE EURA
SLB
OK
STA
BK
KB
AM-NCB
TLF
AL
JS
TS
PA
TB
ATF
HB
OB
BB
KF
KLF
TIBETAN PLATEAU
KJFZ
XSF
LMS
QLS
OT
PACIFIC PLATE
INDIA
SCB
SF
RRF
PHILIPPINE SEA PLATE
SUN
SCS
AS
SS
CS
SUF
FT
WT
70˚ 80˚ 90˚ 100˚ 110˚ 120˚ 130˚ 140˚
60˚ 50˚ 40˚ 30˚ 20˚ 10˚ 0˚
Topography, seismicity, and present-day velocity field
B
50 mm/yr

Figure 1

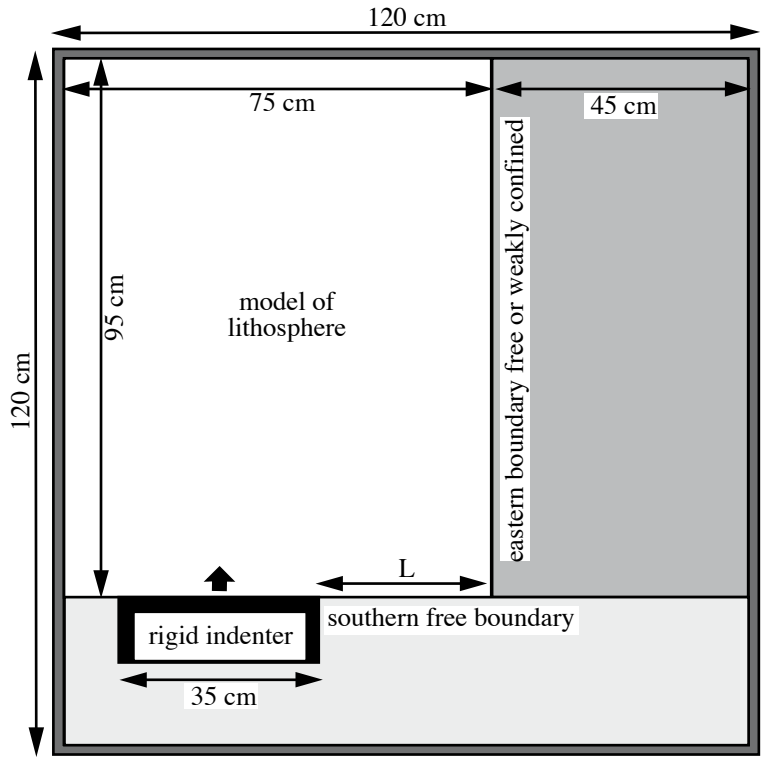
120 cm
75 cm
45 cm
95 cm
model of
lithosphere
eastern boundary free or weakly confined
120 cm
L
rigid indenter
southern free boundary
35 cm

Figure 2

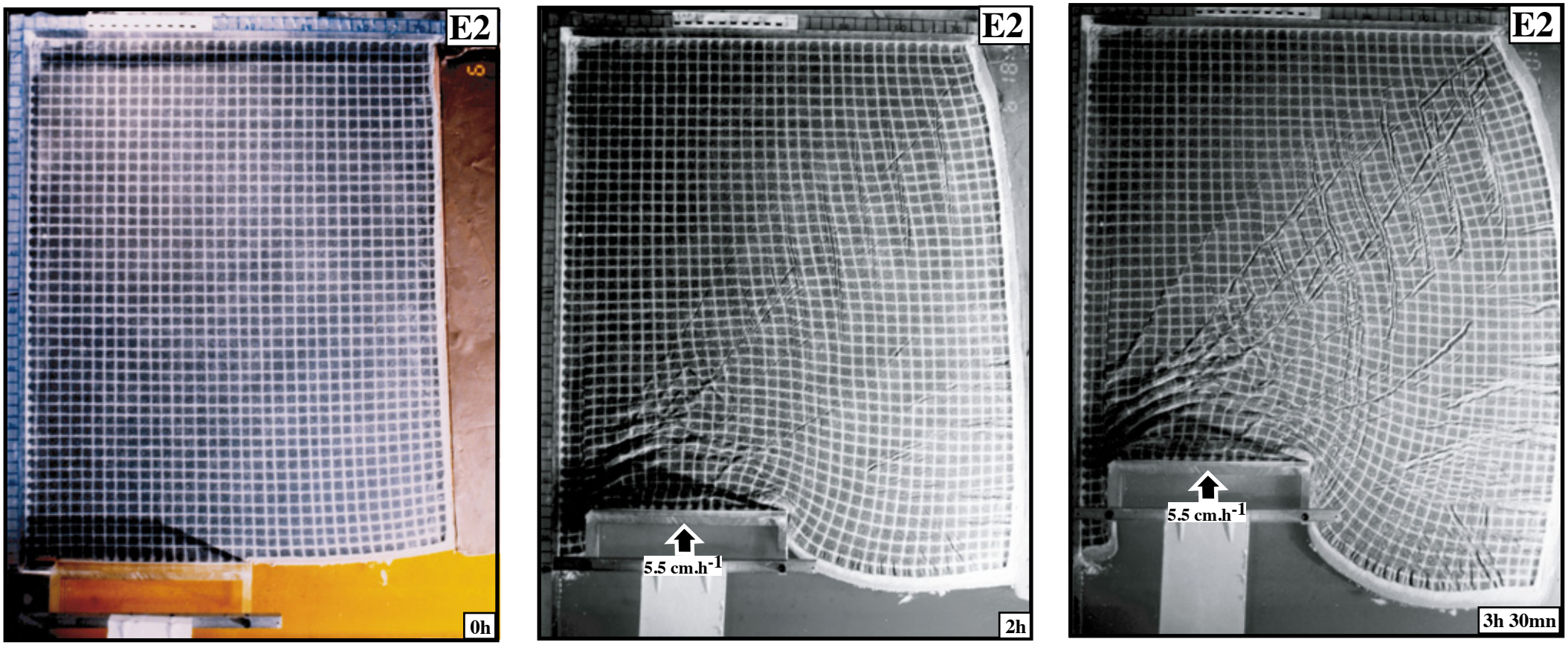

Figure 3

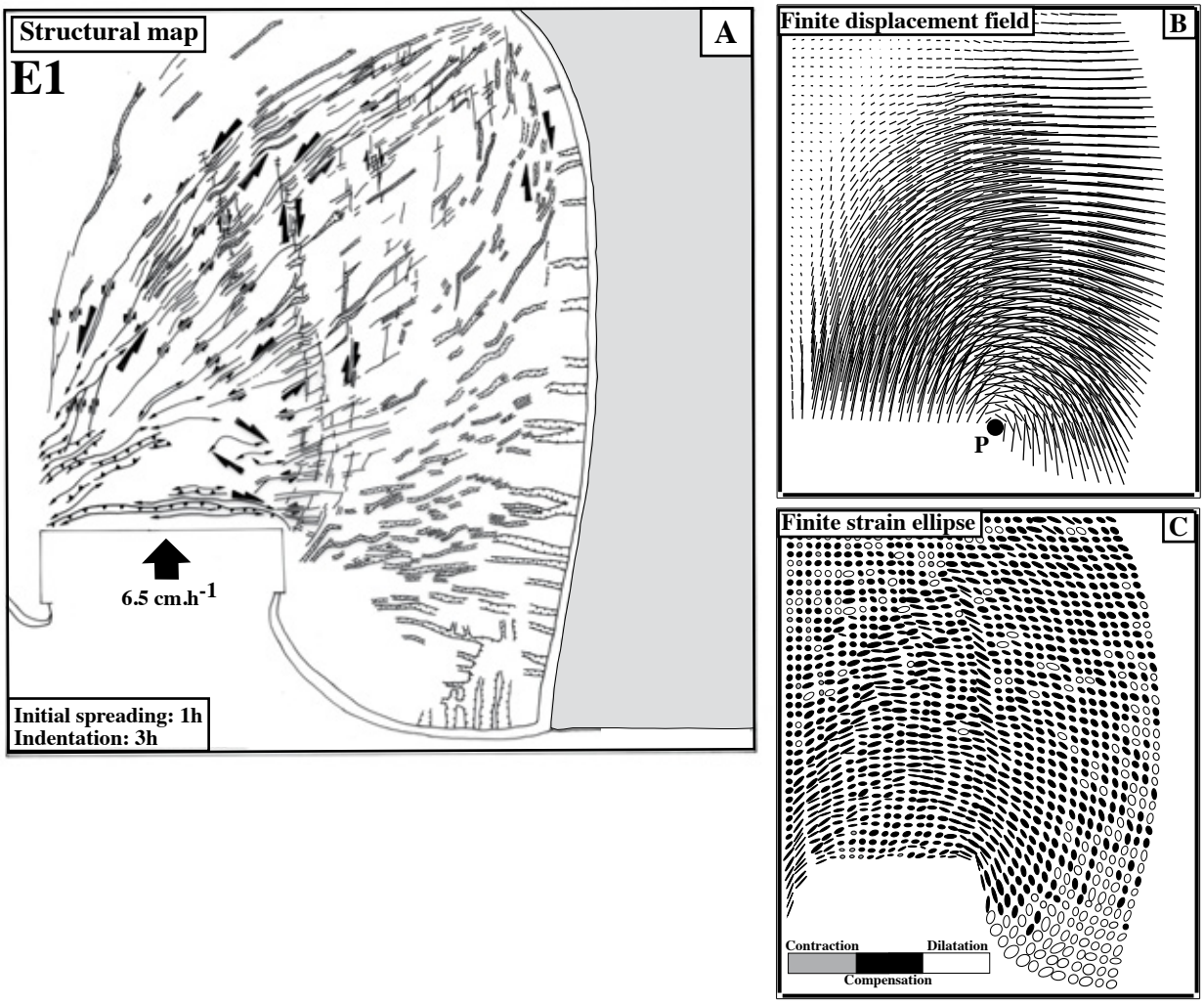
Structural map
E1
A
6.5 cm.h-1
Initial spreading: 1h
Indentation: 3h
Finite displacement field
B
P
Finite strain ellipse
C
Contraction
Dilatation
Compensation

Figure 4

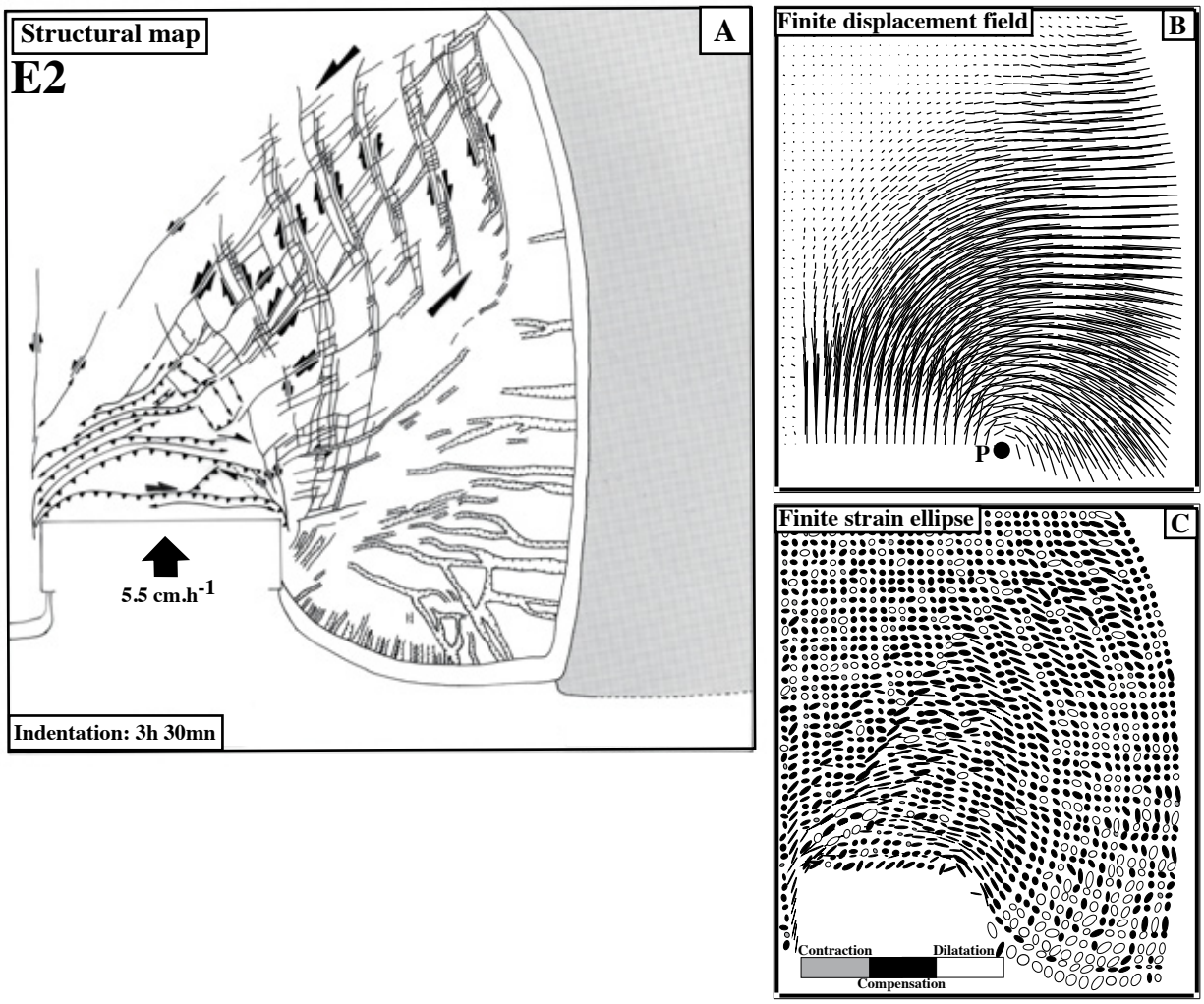
Structural map
E2
A
5.5 cm.h-1
Indentation: 3h 30mn
Finite displacement field
B
P
Finite strain ellipse
C
Contraction
Dilatation
Compensation

Figure 5

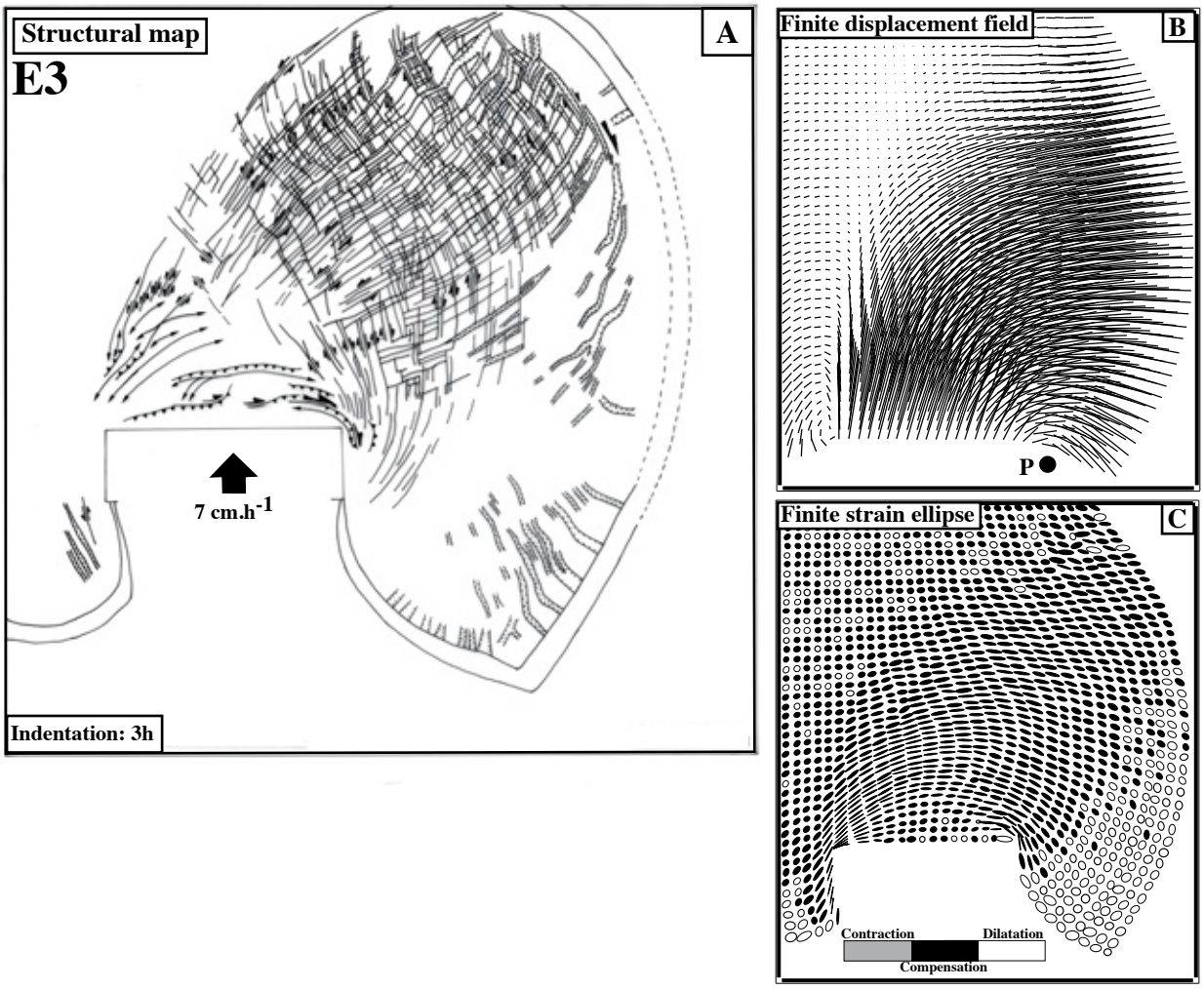
Structural map
E3
A
7 cm.h-1
Indentation: 3h
Finite displacement field
B
P
Finite strain ellipse
C
Contraction
Dilatation
Compensation

Figure 6

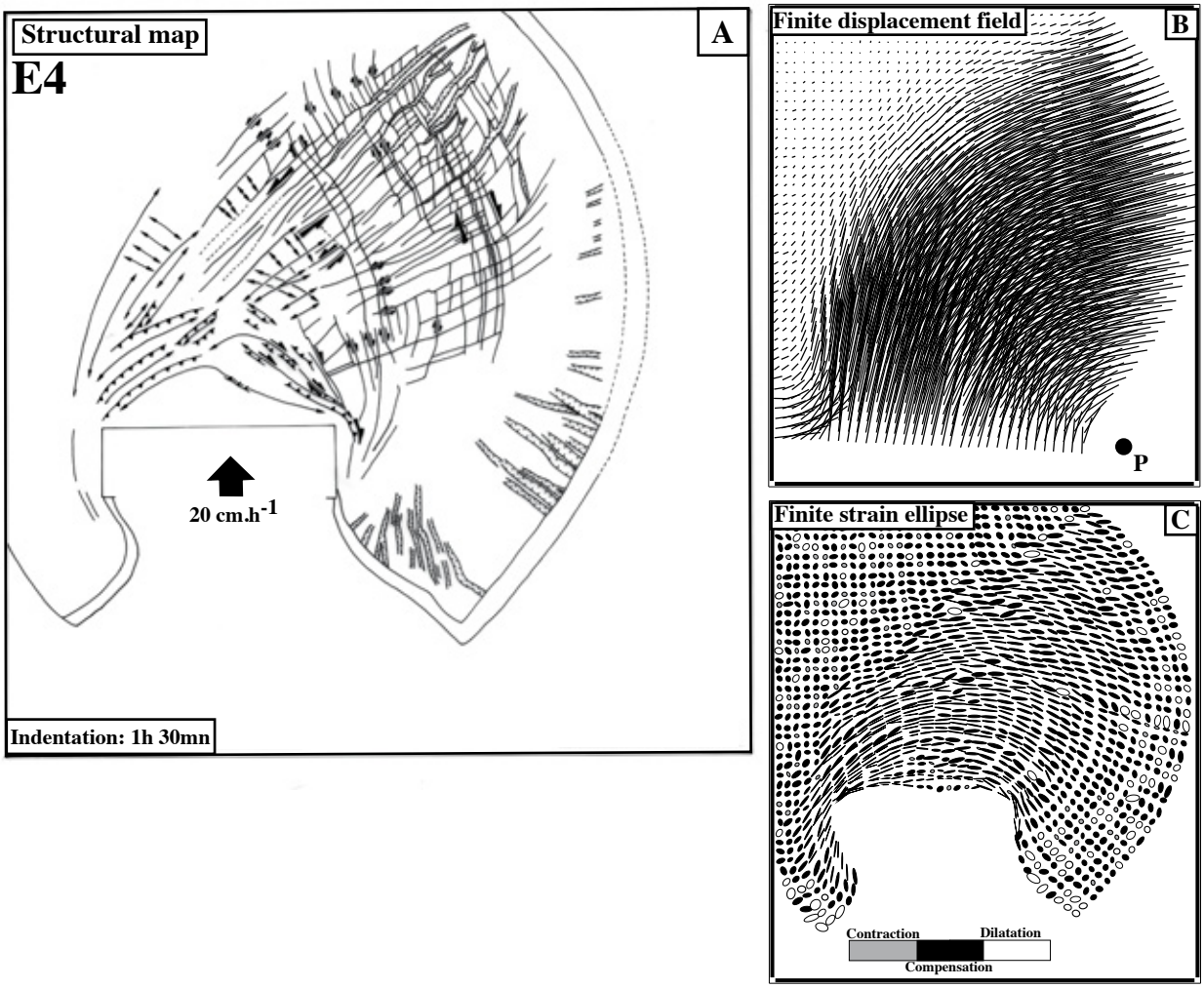
Structural map
E4
A
20 cm.h-1
Indentation: 1h 30mn
Finite displacement field
B
P
Finite strain ellipse
C
Contraction
Dilatation
Compensation

Figure 7

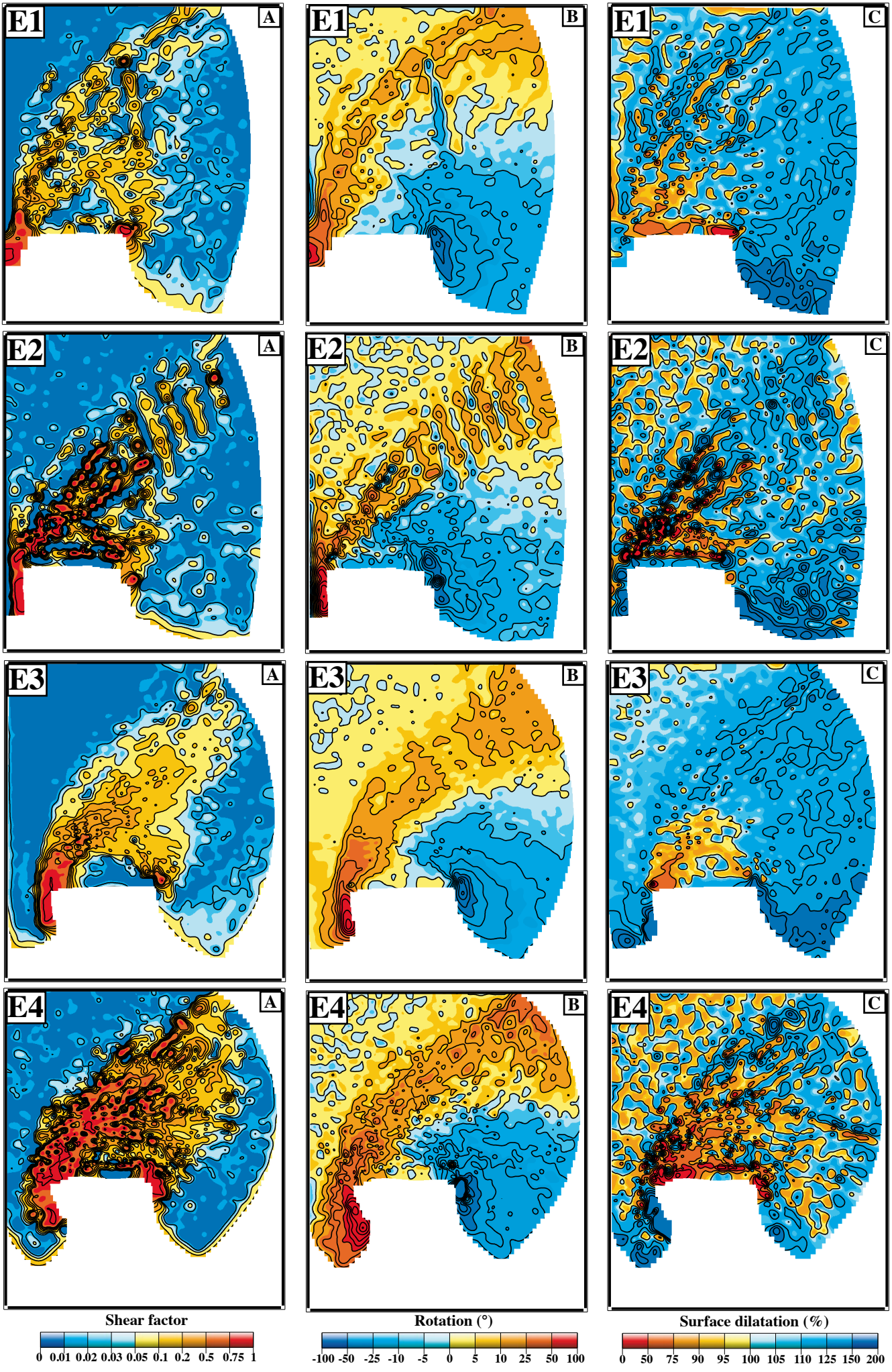
E1
A
E1
B
E1
C
E2
A
E2
B
E2
C
E3
A
E3
B
E3
C
E4
A
E4
B
E4
C
Shear factor
0 0.01 0.02 0.03 0.05 0.1 0.2 0.5 0.75 1
Rotation (°)
-100 -50 -25 -10 -5 0 5 10 25 50 100
Surface dilatation (%)
0 50 75 90 95 100 105 110 125 150 200

Figure 8

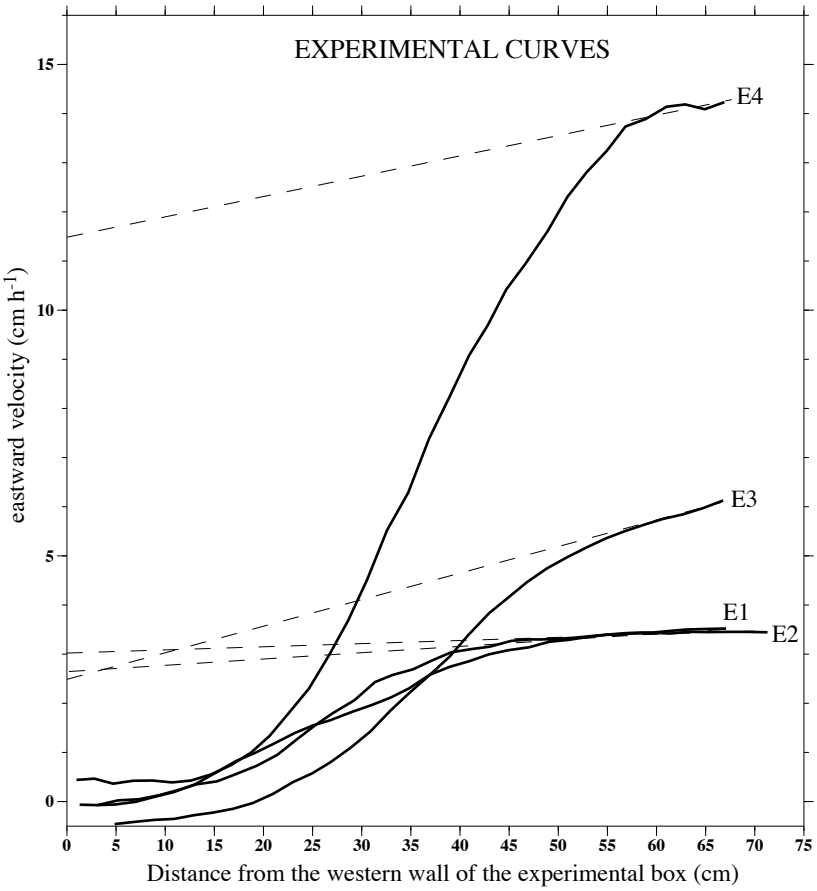
EXPERIMENTAL CURVES
eastward velocity (cm h-1)
15
10
5
0
E4
E3
E1
E2
0
5
10
15
20
25
30
35
40
45
50
55
60
65
70
75
Distance from the western wall of the experimental box (cm)

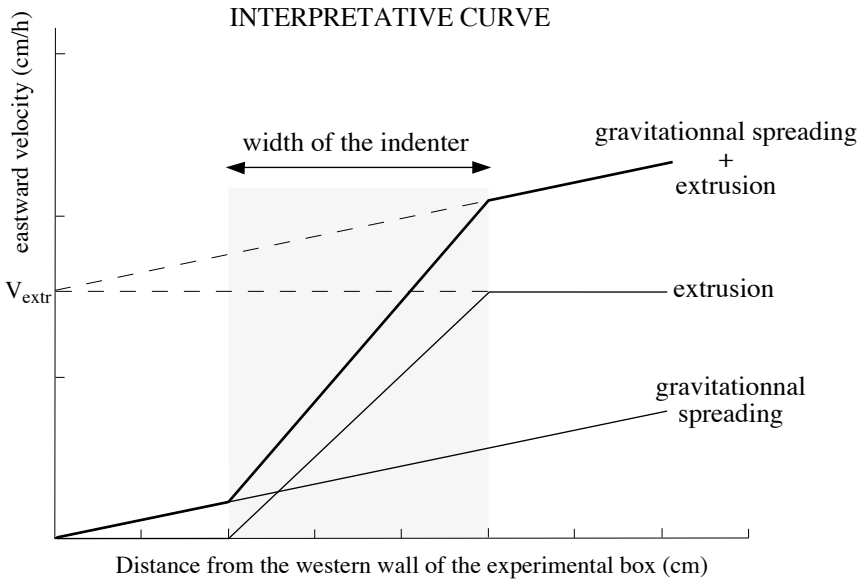
INTERPRETATIVE CURVE
eastward velocity (cm/h)
width of the indenter
gravitationnal spreading
+
extrusion
Vextr
extrusion
gravitationnal
spreading
Distance from the western wall of the experimental box (cm)

Figure 9

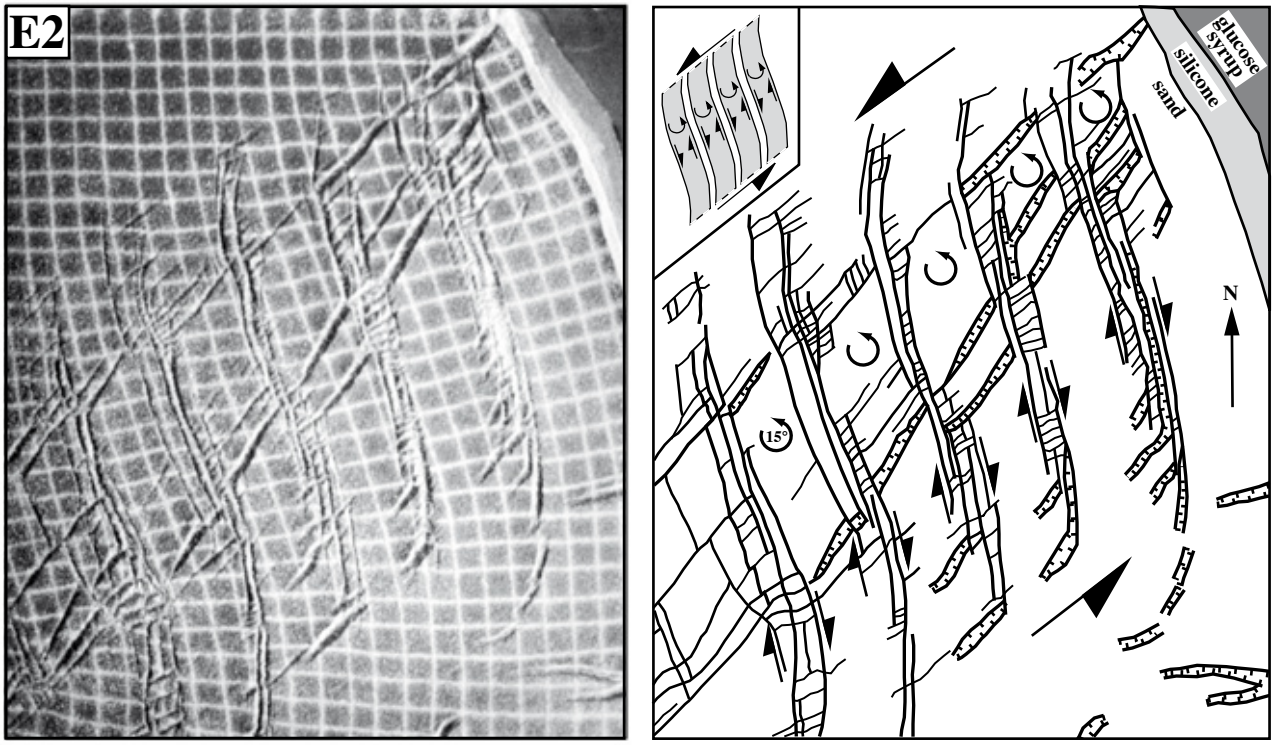

Figure 10

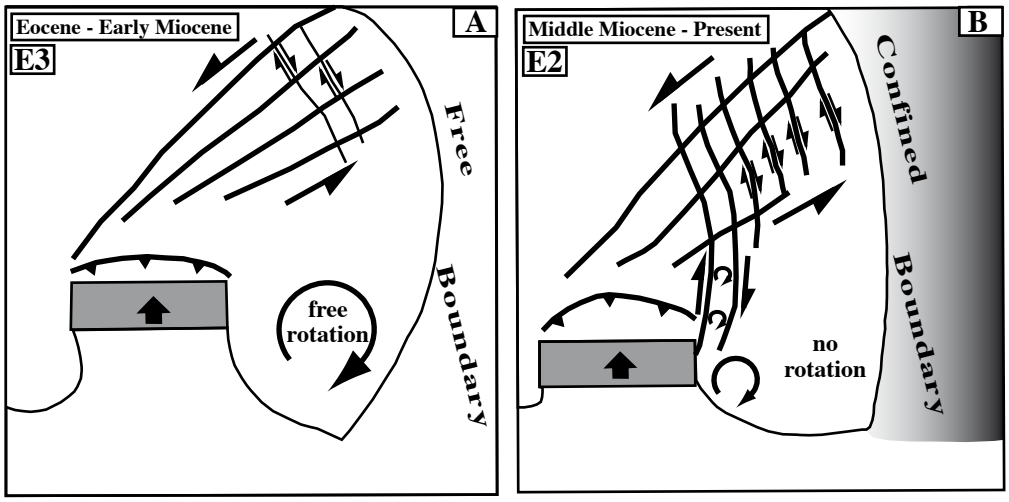
Eocene - Early Miocene
E3
A
Free
Boundary
free
rotation
Middle Miocene - Present
E2
B
Confined
Boundary
no
rotation

Figure 11